# *In vitro* evaluation of different prevention and decontamination strategies used in peri-implant infections of titanium dental implants

**PhD Thesis**

**Roland Masa DMD**


**2023**

**Szeged**

# *In vitro* evaluation of different prevention and decontamination strategies used in peri-implant infections of titanium dental implants

**Roland Masa DMD**

**University of Szeged, Faculty of Dentistry**

**Department of Oral Biology and Experimental Dental Research**

**Doctoral School of Clinical Medicine, Dental Medicine Program**

**Supervisors:**

**Kinga Turzó MSc, PhD**

**Dental School, Medical Faculty, University of Pécs**

**Krisztina Ungvári DMD, PhD**

**Department of Prosthodontics, Faculty of Dentistry**

**University of Szeged**

## PUBLICATIONS RELATED TO AND INCLUDED IN THE THESIS

I. **R. Masa**, Á. Deák, G. Braunitzer, Zs. Tóth, J. Kopniczky, I. Pelsőczi-Kovács, K. Ungvári, I. Dékány, K. Turzó: $TiO_2$/Ag–$TiO_2$ Nanohybrid Films are Cytocompatible with Primary Epithelial Cells of Human Origin: An In Vitro Study. *Journal Of Nanoscience And Nanotechnology* 18 : 6 pp. 3916-3924. , 9 p. (2018), PMID: 29442727, doi: 10.1166/jnn.2018.15261

**IF: 1.093**

II. **R. Masa**, I. Pelsőczi-Kovács, Z. Aigner, A. Oszkó, K. Turzó, K. Ungvári: Surface Free Energy and Composition Changes and Ob Cellular Response to CHX-, PVPI-, and $ClO_2$-Treated Titanium Implant Materials, *Journal of Functional Biomaterials* 13 : 4 Paper: 202, 11 p. (2022) PMID: 36412843, doi: 10.3390/jfb13040202

**IF: 4.901**

**∑IF: 5.994**

## PUBLICATIONS RELATED TO, BUT NOT INCLUDED IN THE THESIS

I. HH. Niller, **R. Masa**, A. Venkei, S. Mészáros, J. Minárovits: Pathogenic mechanisms of intracellular bacteria. *Current Opinion in Infectious Diseases*, 2017; 30:309-315, doi:10.1097/QCO. 0000000000000363

**IF: 3.782**

## TABLE OF CONTENTS

## ABBREVIATIONS

| | |
|---|---|
| **AB** | AlamarBlue® |
| **Ag** | silver |
| **AgNPs** | silver nanoparticles |
| **Ag-$TiO_2$** | silver-titanium dioxide |
| **$Al_2O_3$** | aluminium oxide |
| **BIC** | bone-to-implant contact |
| **BSP** | bone sialoprotein |
| **Ca** | calcium |
| **CA** | citric acid |
| **CHX** | chlorhexidine digluconate |
| **$ClO_2$** | chlorine-dioxide |
| **$CO_2$** | carbon-dioxide |
| **CP** | commercially pure |
| **DMEM** | Dulbecco's modified essential medium |
| **ECM** | extracellular matrix |
| **EDTA** | ethylenediamine-tetraacetic acid |
| **EMEM** | Eagle's minimal essential medium |
| **FBS** | fetal bovine serum |
| **Fe** | iron |
| **GBR** | guided bone regeneration |
| **·OH** | hydroxyl radical |
| **$H_2O_2$** | hydrogen peroxide |
| **HA** | hydroxyl apatite |
| **HCl** | hydrogen chloride |
| **HFO** | human fetal osteoblast |

| | |
|---|---|
| **$IC_{50}$** | half maximal inhibitory concentration |
| **KSFM** | keratinocyte serum-free medium |
| **LDH** | Lactate dehydrogenase |
| **MI** | diiodomethane |
| **MTT** | 3-(4,5-dimethylthiazol-2-yl)-2,5-diphenyltetrazolium bromide |
| **N** | nitrogen |
| **Nd:YAG** | neodymium-doped yttrium aluminum garnet |
| **Ni-Ti** | nickel-titanium |
| **$O_2$** | oxigen |
| **$O_2^-$** | superoxide anion |
| **Ob** | osteoblast |
| **OD** | optical density |
| **OPN** | osteopontin |
| **OWRK** | Owen-Wendt-Rabel-Kaelble |
| **P** | phosphorus |
| **p(EA-co-MMA)** | poly(ethyl-acrylate-co-methyl-methacrylate) |
| **PBS** | phosphate buffered saline |
| **PCR** | polymerase chain reaction |
| **PEO** | plasma electrolytic oxidation |
| **PVPI** | povidone-iodine |
| **PW** | purified water |
| **Ra** | Average roughness |
| **ROS** | reactive oxygen species |
| **S** | sulfur |
| **SDS** | sodium dodecyl sulfate |
| **SEM** | scanning electron microscope |
| **SE** | standard error of the mean |

| | |
|---|---|
| **SFE** | surface free energy |
| **SLA** | sandblasted and large-grit acid etched |
| **Ti** | titanium |
| **$TiO_2$** | titanium dioxide |
| **$Ti_P$** | titanium polished |
| **$Ti_{SA}$** | titanium sandblasted-acid etched |
| **Ti6Al4V** | titanium-aluminium-vanadium |
| **Ti6Al7Nb** | titanium-aluminium-niobium |
| **$TiO_2$ NPs** | titanium dioxide nanoparticles |
| **TNT** | titanium nanotubes |
| **TRITC-phalloidin** | phalloidin–tetramethylrhodamine B isothiocyanate |
| **UV** | ultra violet |
| **wt%** | weight percent |
| **XPS** | x-ray photoelectron spectroscopy |

# 1. INTRODUCTION

Solving the challenges posed by an aging society is one of the primary concerns in the 21st century. The increasing number of elderly individuals necessitates continuous advancements in medical devices and pharmaceuticals to enhance their quality of life. Recent epidemiological studies project that by 2050, approximately 22% of the population will be aged 60 or above [1]. The rehabilitation of partially or completely edentulous patients has undergone a significant transformation, shifting away from traditional treatments like bridges and removable dentures towards dental implants, driven by the discovery of osseointegration [2, 3]. Osseointegration, as described by Brånemark, represents a direct, structural, and functional connection between the implanted material and living bone tissue, without the presence of a fibrous layer. This adaptive relationship is crucial, especially in accommodating the forces generated during mastication [4].

## 1.1 Titanium and its alloys as dental implant materials

Due to its exceptional physical-chemical and mechanical attributes, titanium (Ti) has established itself as the preferred material in orthopedic and dental implantology [5]. Titanium offers several advantages, including a low density (4.51 g/cm³), a low modulus of elasticity, a high strength-to-weight ratio, low thermal conductivity, high corrosion resistance, and remarkable biocompatibility [6]. In fact, untreated titanium alloys are classified as bioinert materials, similar to zirconia, $Al_2O_3$ ceramics, tantalum and niobium. These materials exhibit minimal interaction with surrounding tissues and body fluids, causing no foreign body reaction [7]. The high corrosion resistance and bioinert nature arise from the rapid formation of a protective oxide layer on the surface when exposed to air or water [5]. This layer, initially about 1-5 nm thick, can develop within 30 milliseconds and mainly comprises titanium dioxide ($TiO_2$). $TiO_2$, the outermost layer, is responsible for the material's favorable biological properties [8].

Various grades of pure titanium have been produced for dental applications, categorized from Grade 1 to Grade 4 based on increasing weight percentages (wt%) of Fe (0.2-0.5 wt%) and $O_2$ (0.18-0.4 wt%) [9]. These minor variations in element concentration significantly influence the metal's mechanical properties. The screw-shaped implant body, the part that remains embedded in the bone, is typically crafted from commercially pure Ti (CP 1-4), with

CP2 and CP4 being commonly used. Alloying titanium with other metals further enhances its mechanical properties. Grade 5 (Ti6Al4V) is often chosen as the material for abutments and screws. Notable titanium alloys include Ni-Ti, utilized in endodontics and orthodontics due to its excellent shape memory, and Ti6Al7Nb, employed in surgical (joint replacement) and dental implants [10].

### 1.2 Molecular and cellular events of osseointegration

The long-term success of a dental implant is intricately linked to the quality of osseointegration and the effective prevention of bacterial infiltration from the oral environment. Osseointegration primarily involves the process of new bone formation on and around the implant, regulated by osteoprogenitor and osteoblast cells. The establishment of a gingival seal depends on the proper attachment of gingival epithelial and fibroblast cells.

Many of the molecular and cellular processes at the bone-biomaterial interface have been extensively discussed [11]. When a sterile implant comes into contact with blood, saliva, or tissue fluids, the immediate adsorption of various proteins occurs. Despite the stable oxide layer of the biomaterial, electrochemical changes take place. Elements such as calcium (Ca), phosphorus (P), and sulfur (S) can be incorporated into the oxide layer, while titanium (Ti) ions are released from the surface into adjacent tissues. This subtle release of metal ions could potentially inhibit osteocalcin secretion and the matrix formation of osteoblast cells [12]. In the initial days, the bone-implant interface is predominantly populated by inflammatory cells, specifically neutrophil granulocytes. A collagen-free interfacial zone forms on the surface, known to be rich in osteopontin (OPN) and bone sialoprotein (BSP). These non-collagenous proteins play a crucial role in connective tissue cell adhesion and subsequent matrix mineralization by providing binding sites for calcium phosphate deposition. The ingrowth of capillaries and collagen produced by fibroblasts contributes to the formation of fibrotic callus. In the second stage, osteoprogenitor cells further differentiate into osteoblasts, initiating the development of reticular bone (2-6 weeks). At this point, the absence of micro movements is critical to prevent fibroblast differentiation into fibrocyte cells. The immature bone formed during this phase exhibits irregularly oriented lamellae. Subsequently, in the lamellar bone formation stage (6-8 weeks), further mineralization and the differentiation of osteoblasts into osteocytes occur. The final phase of osseointegration involves the development of mature bone and its adaptation to physiological loading, a process known as remodeling [13].

Gingival attachment around the implant neck serves as a protective barrier for deeper tissues, safeguarding the bone-implant interface against bacteria and other microorganisms. Complete gingival closure typically occurs within one week following surgery, while the establishment of a mature epithelial barrier takes approximately two months [14]. The epidermis of the gingiva comprises three distinct layers of stratified squamous epithelial cells: gingival, sulcular, and junctional epithelial cells. The basal lamina is a mucopolysaccharide-rich binding layer produced by junctional epithelial cells to facilitate adhesion to the implant surface. Our method for isolating gingival epithelial cells has been previously described by Ungvári et al. [15]. Primary epithelial cells exhibit diverse cellular morphology, tend to form groups, and have a slower proliferation rate until they reach confluence. They exhibit a preference for smooth surfaces ($Ra < 0.5$ μm) over rough ones [16, 17]. Due to their sensitivity to changes in culture conditions or target surfaces, primary epithelial cells are ideal for *in vitro* testing of soft tissue responses.

The mucosal attachment around implants and natural teeth shares similarities, but there are significant differences, particularly in the connective tissues. In mucosal attachment around implants, collagen fibers and fibroblast cells are oriented parallel to the implant or abutment surface, whereas in natural teeth, these fibers anchor perpendicularly into the cementum. Reduced cell numbers and diminished blood supply can contribute to the faster and deeper progression of peri-implant infections [14].

In the absence of periodontal ligaments, bone cells establish direct connections with the implant surface. The main types of bone cells involved in osseointegration and bone remodeling processes include osteoblasts, osteocytes, and osteoclast cells. Primary human osteoblast cells are mesenchymal proliferating cells with an average diameter of 10-20 μm. They are responsible for secreting the extracellular matrix (ECM), growth hormones, and cytokines. These cells serve as relevant models for studying bone-biomaterial interactions *in vitro*. However, their heterogeneous phenotype, limited accessibility, and lengthy isolation process have led to the broader application of cell lines [18]. Osteoblast cells transition into osteocytes once they cease proliferating in mineralized bone tissue. Freshly isolated primary osteoblast cells were used in cytocompatibility studies involving chemically treated titanium in the second part of my thesis. The identification of osteoblast cells was conducted through real-time PCR tests and the staining of calcium deposits (Figure 1). The detailed process of primary osteoblast cell isolation, refined by our research group, will be discussed in the following section.

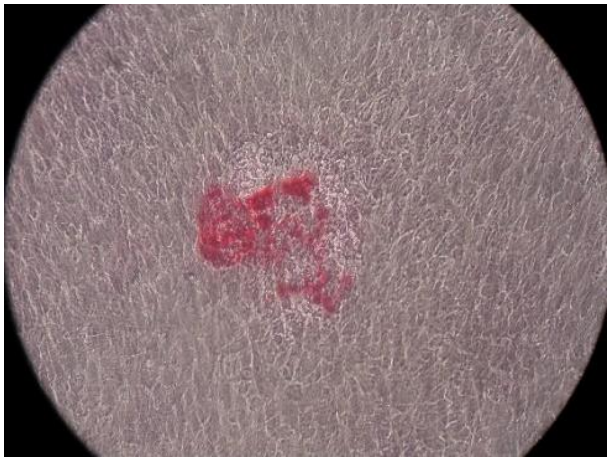

**Figure 1.** Incipient matrix mineralization demonstrated by staining with alizarin red after 3 weeks of incubation. Confluent, multi-layered osteoblasts under light microscope at a magnification of × 100.

The MG-63 osteosarcoma cell line is among the most widely used cellular models for *in vitro* studies related to osseointegration [19]. While this tumor cell line is arrested in the pre-osteoblast stage and may not be ideal for assessing alkaline phosphatase activities, its similarity to primary osteoblasts in terms of integrin subunit profiles, osteocalcin production, ability to provide an unlimited number of cells, and relatively straightforward culture conditions make it an attractive model for investigating the *in vitro* osteoblastic phenotype [18, 20].

### 1.3 Surface modifications of Ti implants

The root form geometry of dental implants is widely accepted, and as a result, the focus of development has shifted toward enhancing the surface properties of these implants. With a growing patient demand for shorter healing times, the primary objective is to enhance the biocompatibility of titanium implants to facilitate quicker osseointegration and more secure gingival closure [21]. In recent years, another emerging trend is the enhancement of antimicrobial properties of implant surfaces, which is becoming increasingly important in light of antibiotic resistance issues [22]. It is important to note that the surface properties of

biomaterials can influence the adsorption of proteins as well as the migration, proliferation, and differentiation of adjacent cells in multiple ways (Figure 2).

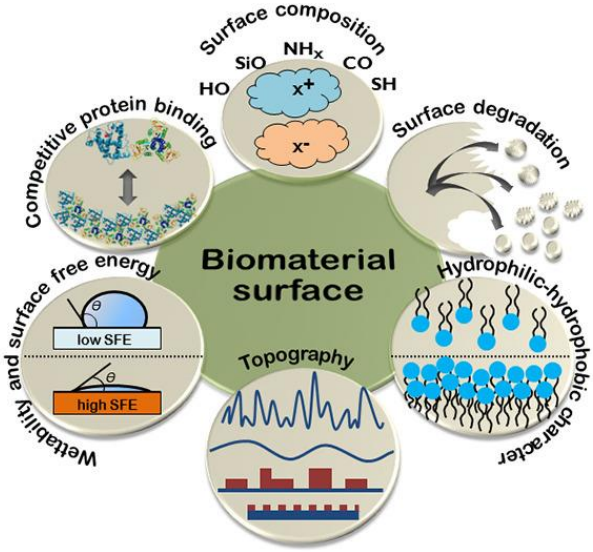


**Figure 2.** Schematic illustration of the main surface parameters and processes in directing cellular responses. Source: Jurak et al. [23]. The figure has been slightly modified.

Implant surfaces can be modified by physico-chemical, morphological, and biochemical methods. However, it is also possible to distinguish between additive and subtractive methods. Additive methods involve surface treatments like impregnating chemicals (e.g., calcium phosphate or fluoride ions) and coating techniques such as titanium plasma spraying, plasma-sprayed hydroxyapatite, and biomimetic coatings (involving peptides, growth factors, and nanomaterials). Subtractive methods, on the other hand, encompass techniques like grinding, blasting, and machining (physical methods), often combined with acid etching (chemical methods). Additionally, ion implantation and laser ablations (including excimer, $CO_2$, and Nd:YAG lasers) are commonly used for improving surface topography [24]. In most *in vitro* and *in vivo* studies, sandblasted and large-grit acid-etched (SLA) titanium surfaces are considered as the control surface, even when compared to newer 3D printed titanium alloys. This preference is due to SLA's proven excellence in promoting osseointegration [25].

### 1.4 Peri-implant infections

While titanium dental implants generally have a relatively high success rate, challenges arise with early failures (before osseointegration) and especially late failures (after

osseointegration) [26]. Changes in the oral microbiome, particularly an imbalance favoring pathogenic bacteria, can lead to inflammation in peri-implant tissues, akin to gingivitis and periodontitis around natural teeth [14]. In both scenarios, anaerobic Gram-negative bacteria dominate the biofilm, although occasionally members belonging to the genera *Peptostreptococcus* or *Staphylococcus* may be detected in peri-implant lesions [27].

Peri-implant mucositis is a reversible inflammation of the soft tissues surrounding the implant, characterized by swelling, redness, bleeding upon gentle probing, and occasional suppuration. This condition is often considered a precursor to peri-implantitis [28] and can be caused by factors such as biofilm accumulation on the implant surface (resulting from poor oral hygiene), smoking, systemic disorders, or radiotherapy. Effective conservative treatment includes professional mechanical debridement, patient motivation and education, along with the use of local antiseptics [29].

Peri-implantitis, on the other hand, is a more aggressive, rapid, and irreversible condition affecting both soft and hard tissues around the implant [30]. Symptoms include bone loss around osseointegrated implants in function, deep probing depths (> 4mm), bleeding, and suppuration. Typically, patients do not report pain, but increased mobility of the implant is a clear sign of advanced peri-implantitis, often leading to implant failure. The disease can be attributed to bacterial infection, implant overloading, fractures, cement residues, or micro gaps [31].

As there is currently no universally accepted gold standard treatment for peri-implantitis, the emphasis should primarily be on prevention. The approach to managing peri-implantitis typically involves a combination of conservative methods, such as mechanical debridement, local or systemic antibiotics, laser therapy, and photodynamic therapy, or surgical interventions, including resective or regenerative procedures. The choice of treatment often relies on individual preferences rather than established scientific protocols [29, 32].

The prevalence of peri-implant mucositis and peri-implantitis has shown significant variation across studies (ranging from 5% to 63.5%), mainly due to inconsistent diagnostic criteria and varying study characteristics. However, on average, reported prevalence rates for peri-implant mucositis and peri-implantitis stand at approximately 43% and 22%, respectively, and these numbers have demonstrated an upward trend over time [33, 34].

## 1.5 Photocatalytic antibacterial coatings

Most of the surface modifications discussed earlier have primarily targeted the microscale range (1-1000 μm). However, recent advancements are increasingly focused on the nanoscale (1-100 nm) [35]. Nano engineering is an emerging field that holds great promise for enhancing the bioactivity of dental implants, and numerous combinations of micro and nano-scale modifications to Ti implants have been reported [36].

One notable approach is the development of photocatalytic antibacterial surfaces or coatings, which have the potential to prevent the initial attachment of pioneering colonizing bacteria, inhibit biofilm formation, and reduce pathogenic bacterial loads by releasing reactive oxygen species (ROS) [22, 37, 38]. Titanium dioxide and silver-doped titanium dioxide nanoparticles (Ag-$TiO_2$) embedded in a polymer matrix can be applied as innovative antibacterial surface coatings on Ti surfaces.

Due to its chemical inertness, low toxicity, and high photoactivity, titanium dioxide is one of the most widely used photocatalysts in industrial and medical applications [39, 40]. $TiO_2$ nanoparticles ($TiO_2$NP) have been successfully integrated into various dental materials, including endodontic sealers, veneers, crowns, acrylic resin dentures, restorative composites, ceramics, and whitening agents [41].

The photocatalytic property of $TiO_2$ for splitting water was first reported in 1972 [42]. Being a semiconductor, $TiO_2$ can be excited by irradiation with high-energy photons (UV light) under aerobic conditions, causing an electron to move from its valence band to the conduction band. This process generates a positive hole in the valence band, and the resulting electron-hole pair can interact with atmospheric water ($H_2O$) and oxygen ($O_2$), leading to the production of reactive oxygen species (ROS), including the superoxide anion ($O_2^-$), hydroxyl radical (OH), and hydrogen peroxide ($H_2O_2$) [43]. It is important to note that the lifetime of these radicals is extremely short, on the order of femto- and picoseconds [44], and they play a role in destroying adsorbed bacterial biofilms through various mechanisms [45].

However, due to its relatively large band gap energy (3.2 eV), $TiO_2$ can only be excited by UV light, limiting its practical use with human tissues. Nevertheless, it is possible to shift its light absorption into the visible range by introducing metallic (Ag) and non-metallic elements [46, 47].

Metallic silver, silver salts, and silver nanoparticles (AgNPs) are commonly used antibacterial agents, although their bactericidal effects are sometimes overestimated, while their cytocompatibility is underestimated [48]. The small size of AgNPs (typically < 100 nm) and their large surface-to-volume ratio make them attractive antimicrobial agents with properties that can combat bacteria, viruses, and fungi. Various mechanisms, including intracellular processes [49] and direct contact-based elimination of bacteria, have been reported [50] (see Figure 3).

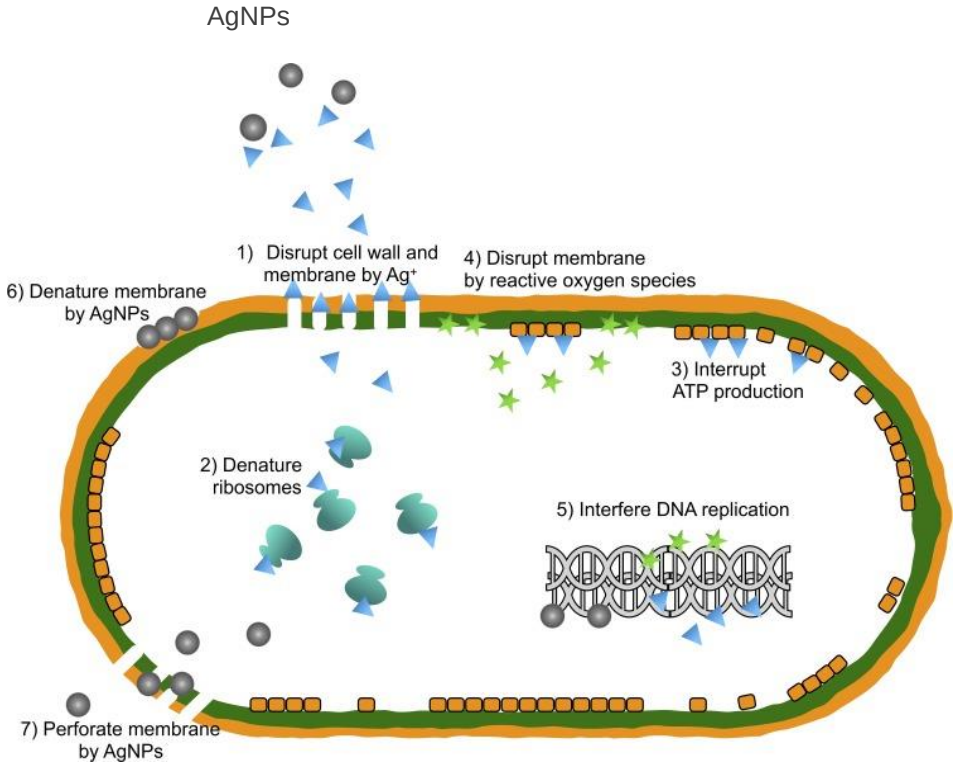


**Figure 3.** Different ways of antibacterial actions of silver nanoparticles (AgNPs). Persistent release of silver ions is responsible for the perforation of cell wall, and interaction with intracellular components. Source: Yin et al. [49]. The figure has been slightly modified.

Silver nanoparticles (AgNPs) are widely used in various dental applications, but their potential use in implant dentistry has not been extensively explored. Despite concerns about the potential toxicity of AgNPs, no systemic toxicity has been reported [49]. Coatings of titanium-silver (0.7-9%) on titanium surfaces have demonstrated effective antibacterial properties without causing cytotoxicity in epithelial and osteoblast cell lines [51]. Besinis et al. described potent antibacterial nano-silver coatings on titanium [52].

The addition of nano-silver to $TiO_2$ can enhance its photocatalytic activity under visible light. Our research group has developed new poly-acrylate resin-based $TiO_2$ and Ag-$TiO_2$ nano-

hybrid films through photodeposition [53]. While these films were initially designed as self-cleaning systems, their promising antibacterial properties, along with mechanical stability, suggest potential dental applications. After 60 minutes of UV irradiation, partial degradation of the polymer bed was observed, leading to higher photocatalyst concentration on the outermost part of the coatings. The disinfectant effect primarily relies on the photocatalytic property of Ag-modified nanohybrid films rather than the bactericidal effect of released silver ions [54]. $TiO_2$-copolymer coatings applied to titanium under visible light illumination and Ag-$TiO_2$-copolymer films (with 0.5% Ag content) in dark conditions exhibited excellent antimicrobial properties against *S. salivarius* [55].

Based on our preliminary studies, we reduced the Ag content in the polymer films from 0.5% to 0.001% to improve cellular compatibility. Venkei et al. reported the high efficacy of $TiO_2$- and Ag-$TiO_2$ nano-hybrid films (with 0.001% Ag content) in eliminating *S. mitis* [56]. Inhibiting bacterial attachment could help to prevent peri-implant infections, and photoactivation with LED light (commonly used in dental polymerization lamps) followed by ROS formation could serve as a primary therapy for peri-implant infections. The challenge lies in finding a biologically well-tolerated concentration of these nanoparticles.

### 1.6 Decontamination of the infected implant side

Much like natural teeth, the biofilm that forms on implant surfaces is a well-organized and mechanically stable community of various bacteria. While the qualitative composition of the biofilm and the immune system's response are similar to those around natural teeth, the progression of biofilm-related issues is more aggressive in the case of peri-implant tissues [57]. A common step in both conventional and surgical therapies is mechanical debridement, which involves the use of titanium or plastic curettes or air-powder abrasives [58]. However, decontaminating titanium surfaces is challenging due to their macro and micro-topography. These surface irregularities, designed to promote better osseointegration, also provide shelter for bacteria to survive. Therefore, chemical agents are often preferred as supplemental tools by most clinicians. Sterile saline, chlorhexidine (CHX), citric acid (CA), hydrogen peroxide ($H_2O_2$), ethylene-diamine-tetra-acetic acid (EDTA), chloramine-T, and local antibiotics are frequently used to disrupt biofilm and eliminate toxins/residues from the implant surface [59-61]. However, many of these agents have drawbacks, and a globally accepted consensus regarding a precise protocol for peri-implant diseases is still lacking [59].

Chlorhexidine digluconate has been well-documented for its antimicrobial efficacy in both periodontal and peri-implant infections [62, 63]. CHX possesses nonspecific, broad-spectrum antibacterial, antifungal, and antiviral activity, as well as high affinity for adsorption to soft and hard tissues (substantivity). It reduces plaque formation and destroys bacteria by disrupting their cell walls and causing lysis [64]. The behavior of CHX, whether bacteriostatic or bactericidal, depends on its concentration. Various forms of CHX, including mouth rinse, toothpaste, varnishes, and gels, are produced in concentrations ranging from 0.02% to 2% [65]. The Anti-Discoloration System of Curasept can inhibit the staining side effects typically associated with other CHX solutions [66]. To date, bacterial resistance against CHX has not been reported [67]. However, recent studies have not recommended the use of CHX as an implant decontamination agent due to concerns about its unclarified cytotoxicity to osteoblasts [68].

Povidone iodine (PVPI) also exhibits rapid, broad-spectrum antibacterial and antiviral activity [68], and it can penetrate biofilms. Other beneficial properties of this iodophor include the absence of bacterial resistance, no staining effects, and good cytocompatibility [69]. All the iodine content in Betadine is in a complex form; however, individuals with previous iodine allergies may have relative contraindications [70]. While the use of povidone-iodine as an adjunctive therapeutic agent is not very common, it holds great potential [71, 72].

Solumium is a lesser-known antiseptic solution containing hyper pure chlorine dioxide ($ClO_2$), invented by Noszticzius et al. [73]. The penetration of this antiseptic into human tissues is limited, but it exhibits rapid bactericidal properties based on interactions with crucial amino acids. Superiority of this $ClO_2$ solution in reducing aerobic bacteria and *Candida*, along with comparable efficiency in reducing anaerobic bacteria compared to CHX, has been reported [74]. Other studies have also highlighted the potential of $ClO_2$ as an alternative agent to CHX [75-77]. Bacterial attachment to a sterile implant surface is an event that is almost impossible to avoid during invasive implant placement surgery in the oral cavity. Antibacterial coatings could inhibit the spread of bacteria and should promote the integration of host tissues, including osseointegration and soft tissue sealing. In cases where peri-implant infection develops, the photo-activation of nanoparticle-coupled polymer films, supplemented with chemotherapeutic agents, appears to be an effective combination. However, residues of these agents could alter the physicochemical properties of the titanium surface and subsequent cellular responses [78].

## 2. AIMS OF THE THESIS

The primary goal of my research was to investigate two different strategies employed against inflammation occurring around dental implants. In the first part of my dissertation, I examined two newly developed photocatalytic coatings ($TiO_2$ and Ag-$TiO_2$ copolymer). These polymer coatings could play a significant role in the prevention of peri-implantitis and the conservative (non-surgical) treatment of established inflammation. It is crucial for a biomaterial (such as a titanium dental implant) to maintain high biocompatibility even after surface modification. My colleague, Annamária Venkei, had previously confirmed the antibacterial effects of these polymer films, so our focus was on assessing the biocompatibility of the surfaces before proceeding to more complex animal experiments and clinical studies. Initially, we conducted a physicochemical analysis of the surfaces, followed by an examination of the adhesion and proliferation tendencies of two different cell types (epithelial and osteosarcoma cells).

In the second part of my dissertation, I examined the potential effects of disinfectants applied during the decontamination of titanium dental implants on the titanium surface. Various chemical agents (disinfectants) are routinely used in dental clinics, but the detailed interaction of these agents with titanium surfaces is not yet fully understood. We investigated two widely used solutions (Curasept and Betadine) and a recently developed one (Solumium). Initially, we examined the surface wettability, calculated the surface free energy, and assessed any possible changes in the chemical composition of the surfaces after a 5-minute treatment. To model the body's response, we evaluated the adhesion and proliferation of freshly isolated osteoblast cells.

Our research set out to achieve several key objectives. Firstly, we aimed to conduct a comprehensive physicochemical analysis of nanocomposite films. Secondly, we sought to assess the *in vitro* biocompatibility of these nanocomposite films by examining their interactions with epithelial and osteosarcoma cells. Additionally, we embarked on an investigation into the physicochemical properties of titanium surfaces that had been treated and came into contact with various chemical agents. Lastly, we focused on evaluating the biocompatibility of these chemically treated titanium surfaces, specifically their interactions with primary osteoblast cells.

# 3. MATERIALS AND METHODS

## 3.1 Photocatalytic films on Ti surfaces

### *3.1.1 Preparation of Ti samples*

Titanium sample disks, measuring 1.5 mm in thickness and 9 mm in diameter, were produced from commercially pure titanium rods (Denti® System Ltd., Szentes, Hungary). In dental implantology, commercially pure grade 4 (CP4) titanium is widely utilized due to its unalloyed form, characterized by low levels of N, C, H, Fe and O, which impart crucial physical and mechanical properties [79]. For studies involving epithelial cell culture, disks with a machined surface (Ra < 0.5 μm) were employed, while sandblasted and acid-etched (SA) disks (Ra ~ 1.5 μm) were used for investigations of the MG-63 immortalized cell line. Before the application of spray coating, all samples underwent a cleaning process involving acetone (puriss, Molar Chemicals, Hungary) followed by immersion in 70% ethanol (puriss, Molar Chemicals, Hungary) in an ultrasonic bath for 15 minutes. Subsequently, they were rinsed three times in ultrapure water (Milli-Q® system, Merck, USA) as per our standard protocol for titanium disks. Following this procedure, the sandblasted and acid-etched disks were coated with nano hybrid films.

### *3.1.2 Preparation of $TiO_2$ and Ag-$TiO_2$ copolymer films*

Control samples consisted of polished titanium disks ($Ti_P$) for epithelial cells and sandblasted and acid-etched ($Ti_{SA}$) titanium disks for MG-63 cells. Two distinct photocatalytic layers were investigated: one comprised of 60% $TiO_2$ and 40% copolymer, and the other consisting of 60% $AgTiO_2$ and 40% copolymer, with a silver concentration ([Ag]) of 0.001 m/m %. These nanoparticles were immobilized on the surface using a hydrophilic polyacrylate resin, specifically, poly(ethyl-acrylate-co-methyl-methacrylate) (p(EA-co-MMA)) as the binder material, sourced from Evonik Industries (Germany). The methodology for producing these aqueous suspensions has been elaborated in the study of Veres et al. [53].

Preceding the coating process, the suspensions underwent homogenization for 15 minutes via a sonicator (Elma Hans Schmidbauer GmbH & Co. KG Stuttgart, Germany). Subsequently, they were sprayed onto the titanium disks using an AD-318 spray gun (Alder, USA) at an approximate density of 2 ± 0.05 mg per disk and then subjected to drying at an

elevated temperature of 120 °C (Figure 4). Finally, the disks were sterilized in a hot air sterilizer at 180 °C for 45 minutes. To initiate partial photodegradation of the upper layer of the polymer film, the disks were exposed to UV-C light at 254 nm for 60 minutes, thereby revealing the silver and $TiO_2$ nanoparticles [53].

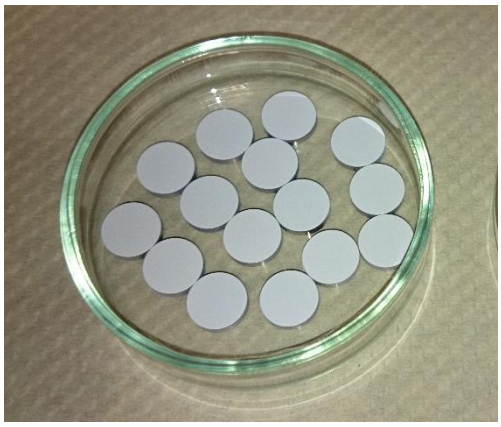

**Figure 4.** $AgTiO_2$ copolymer photocatalytic film covered Ti disks before UV-C irradiation.

### *3.1.3 Scanning electron microscopy*

The surface morphological features of the polymer films were examined in the absence of cells before undergoing UV treatment. To capture high-resolution images, a field emission scanning electron microscope (SEM) (Hitachi S4700, Japan) was employed, operating at magnifications of ×500 and ×5000 in secondary electron imaging mode. For improved image acquisition, the samples were tilted at a 45° angle.

### *3.1.4 Profilometry measurements*

Surface profilometry measurements were conducted using the Veeco Dektak 8 Advanced Development Profiler® (Veeco Instruments, USA). The average surface roughness (Ra, measured in micrometers - μm) of the disks was determined within 500×500 $\mu m^2$ areas. Measurements were recorded at three distinct locations on two samples from each group. During the measurements, the scanning direction maintained a resolution of 0.17 μm with a spacing of 6.33 μm between the scanned lines. The vertical resolution achieved an impressive 4 nm. Furthermore, macro-roughness line profiles were also captured and subsequently analyzed on a computer using the Vision 3D Image and Analysis Software (Veeco Instruments, USA).

### *3.1.5 Cell culture studies*

We investigated two distinct cell culture models: primary human epithelial cells and MG-63 osteosarcoma cells. To obtain adult epidermal epithelial cells, we followed a rigorous protocol. Specifically, these cells were isolated from inflammation-free gingival mucosa, and this process was carried out with the signed informed consent of patients aged over 18 who were undergoing routine dento-alveolar surgery. Our protocol adhered to the principles outlined in the Declaration of Helsinki in every aspect and received approval from the Regional Research Ethics Committee for Medical Research at the University of Szeged (Approval No. 130/2009). The method for primary epithelial cell isolation was comprehensively described in the study conducted by Kitano et al. [80] and has been further refined by our research group. In summary, the procedure involved washing gingiva specimens in Salsol A (sterile isotonic salt solution, Human Rt., Gödöllő, Hungary) supplemented with a 2% antibiotic and antimycotic solution (containing penicillin, streptomycin, and amphotericin B, sourced from Sigma-Aldrich GmbH, Germany). Following an overnight incubation in dispase solution (Grade II, Roche Diagnostics, Germany) at 4°C, the epidermis was easily separated from the dermis using forceps. Subsequently, the epidermis underwent further incubation with a 0.25% trypsin-EDTA solution (Sigma-Aldrich GmbH, Germany) for 5 minutes at 37°C. After vigorous strumming, epidermal cells were released into suspension and then centrifuged at 200g for 10 minutes at 4°C. Following the removal of the supernatant, the cells were diluted with culture medium and transferred into a 25 $cm^2$ flask [15].

The complete culture medium for primary epithelial cells was composed of keratinocyte serum-free medium (KSFM) with L-glutamine (Gibco BRL, Eggstein, Germany). This medium was supplemented with recombinant epidermal growth factor (2.5 μg/500 ml, Gibco BRL, Eggstein, Germany), bovine pituitary extract (25 mg/500 ml, Gibco), and a 1% antibiotic and antimycotic solution.

MG-63 osteoblast-like cells were procured from the European Collection of Cell Cultures. To initiate their culture, one frozen ampoule containing these cells was thawed by placing it in a 37°C water bath for a brief period. Once thawed, the cells were centrifuged in a solution of phosphate buffered saline (PBS) (PAA Laboratories GmbH, Germany) and fetal bovine serum (FBS) (PAA Laboratories GmbH, Germany). MG-63 cells were then transferred into a 25 $cm^2$ flask and underwent at least three passages before being employed in the investigations, mirroring the procedure followed for epithelial cells.

The medium for MG-63 cells consisted of Eagle's Minimal Essential Medium (EMEM) (Sigma-Aldrich GmbH, Germany), which was supplemented with 10% FBS, 1% L-glutamine, 1% nonessential amino acids (Sigma-Aldrich GmbH, Germany), and 1% antibiotic and antimycotic solution. The culture medium was refreshed three times per week, and the cultures were maintained under standard conditions, including a 5% $CO_2$ atmosphere at 37°C, in a humidified thermostat.

For the experiments, cells were pipetted onto the sample disks at a density of $10^4$ cells per well and cultured in 48-well plates. Plate wells were utilized as control surfaces with the same quantity of cells. Cell attachment was assessed after 24 hours, while the proliferation rate was measured after 72 and 168 hours using the 3-(4,5-dimethylthiazol-2-yl)-2,5-diphenyltetrazolium bromide (MTT) assay (Sigma-Aldrich GmbH, Germany). These experiments were replicated four times, and four samples were employed for each assay/group with both cell types. Additionally, MTT measurements were complemented with fluorescent microscopy, with one sample from each group used for cell visualization.

#### *3.1.5.1 MTT assay*

MTT is a rapid colorimetric assay that gauges the quantity of living cells through the reduction of tetrazolium salt facilitated by mitochondrial dehydrogenases [81]. In our study, cells were dispensed into 48-well plates at a density of $10^4$ cells per well and cultured on the sample disks in culture medium for 24, 72, and 168 hours.

Following the respective incubation periods, the culture medium was aspirated and replaced with a 1 mg/ml MTT solution in EMEM/KSFM. After 4 hours of incubation at standard conditions (37°C), this MTT-containing medium was carefully withdrawn from each well. The water-insoluble formazan crystals, a crystallized form of the dye produced by the viable cells, were subsequently dissolved using a solution consisting of 0.04 mM HCl in absolute isopropanol and 10% sodium dodecyl sulfate (SDS).

To measure the optical density at 540 nm ($OD_{540}$), we employed an Organon Teknika Reader 530 spectrophotometer (Anthos Labtec Instruments GmbH, Austria). It is important to note that plate wells without disks were employed as positive controls for this procedure.

#### *3.1.5.2 Visualization with fluorescent microscopy*

Fluorescent dyes were used for the visualization of the cultured cells. Representative images of the disks were taken after definite incubation periods with the cells, in parallel with the colorimetric assay. The cells were fixed on the Ti disks with 4% formaldehyde. Cell nuclei were labeled with Bisbenzimide Hoechst 33342 dye (blue, Merck Millipore, Germany) and the cytoskeleton with Phalloidin–Tetramethylrhodamine B isothiocyanate (TRITC-phalloidin, red, Sigma-Aldrich GmbH, Germany). The images were taken with a Nikon Eclipse 80i fluorescent microscope (Nikon Corporation, Japan) at a magnification of ×100. In each case, two images were taken using two different filters (DAPI, ex. [320], [520] nm; TRITC, ex. [510-560] nm) with the position of the samples unaltered. Final composite pictures were created with ImageJ [1.47v] software (National Institutes of Health, USA).

### *3.1.6 Statistical analysis*

We calculated the means ± SE (standard error of the mean) for Ra (μm) measured by the profilometer and $OD_{540}$ values measured by the plate reader. Subsequently, our data underwent normality testing, and we conducted comparisons using a one-way analysis of variance (ANOVA), followed by post hoc tests including Tukey's HSD, LSD, and Scheffé. All statistical analyses were carried out using SPSS 21 (Chicago, Illinois, USA), and the significance level was established at $p < 0.05$.

## 3.2 Decontamination agents on Ti surfaces

### *3.2.1 Preparation of Ti samples*

Disks made from CP4 titanium rods (Denti® System Ltd. Hungary), measuring 1.5 mm in thickness and 9 mm in diameter, were used in the study. The manufacturer had sandblasted and acid-etched the surface of these disks. Subsequently, the disks were subjected to a cleaning process using acetone and 70% ethanol, following established procedures.

The titanium samples were then exposed to three different chemical decontamination agents for a period of 5 minutes each, which is a practical timeframe commonly used in routine dentistry for easy replication. The decontamination agents used were chlorhexidine-digluconate (Curasept ADS 220, 0.2%, Switzerland), povidone-iodine (Betadine, 10%, Switzerland), and chlorine-dioxide (Solumium dental, 0.12%, Hungary). Following the treatment, the disks were

thoroughly washed with ultrapure water three times. In contrast, control disks were solely rinsed with ultrapure water.

### *3.2.2. Contact angle measurements*

The wetting properties of the treated samples were analyzed using an OCA 20 instrument (Dataphysics, Germany), which employed purified water (PW, pharmaceutical grade, compliant with Ph.Hg. VIII of the European Pharmacopoeia 9.0, as specified by the European Directorate for the Quality of Medicines and HealthCare, France) and diiodomethane (MI, Merck KGaA., Germany) drops. A single measurement was taken for each disk, utilizing drops with a volume of 10 µl placed at a fixed distance of 10 mm from the surface.

In our experiment, we assessed six Ti disks treated with each chemical agent. The results were analyzed using the SCA 20 and 21 software (DataPhysics Instruments GmbH, Germany). The surface free energy (SFE), expressed in γ (mJ/m2), was determined using the Owen-Wendt-Rabel-Kaelble (OWRK) method, a widely used technique in implantology [82, 83].

### *3.2.3 X-ray photoelectron spectroscopy*

Chemical composition of the titanium surfaces was assessed through XPS-LEIS analysis. Photoelectrons were generated using Al Kα primary radiation (hν = 1486.6 eV) and subsequently examined using a hemispherical electron energy analyzer (PHOIBOS 150 MCD 9, SPECS, Germany). The X-ray gun was operated at 150 W (12 kV, 12.5 mA). To standardize the binding energies, they were referenced to the position of the C 1s peak originating from adventitious carbon, which was defined as 285.1 eV. Both wide-range scans and high-resolution narrow scans of the characteristic peaks for Ti 2p, O 1s, and C 1s were recorded [84, 85].

### *3.2.4 Cell culture studies*

Our research team has modified the protocol for isolating primary oral human osteoblast cells [86]. Bone chips were collected from healthy adult patients who underwent routine dento-alveolar surgery and did not have any common illnesses. Osteoblast cells were extracted from small bone fragments that were removed during the surgical extraction of wisdom teeth, with the written consent of the patients. This study protocol fully adhered to the principles outlined

in the Declaration of Helsinki and received approval from the Regional Research Ethics Committee for Medical Research at the University of Szeged (Approval Number: 188/2013).

Before the enzymatic digestion process, the bone chips were thoroughly rinsed with aqueous solutions of Salsol A and a 4% antibiotic-antimycotic solution (Corning, USA) multiple times (Figure 5). To release cells from the bone fragments, the samples were incubated in a mixture of collagenase type II (1 mg/ml, MP Biomedicals, USA) and trypsin (0.25%) - EDTA (PAN-Biotech GmbH, Germany), following our modified protocol [86]. The culture medium used was Dulbecco's Modified Essential Medium (DMEM) (Corning, USA). Primary osteoblast cells were passaged at least three times before being used in experiments.

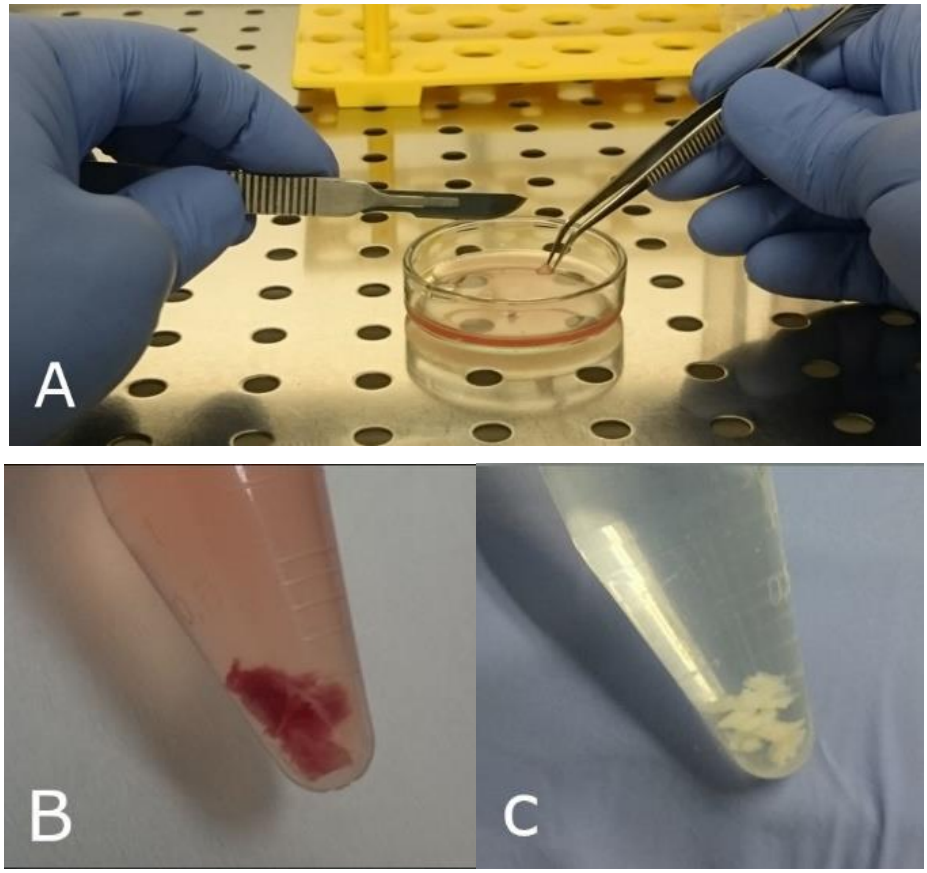


**Figure 5.** Preparation of bone chips with a forceps and a scalpel (A). Smaller fragments before (B) and after (C) multiple vortex and washing in PBS.

Cells were seeded onto the titanium (Ti) disks at a density of $10^4$ cells per well and cultured in 48-well plates designed for sensitive assays. In this context, the wells of the plates (referred to as "plate") were employed as a positive control group, which did not contain any Ti disks. Cell attachment was assessed after a 24-hour period, while the proliferation rate was measured after 72 hours. These experiments were conducted in triplicate, and each assay

utilized four samples. To evaluate cellular responses, we employed standard colorimetric assays (MTT, alamarBlue®, lactate dehydrogenase (LDH) test), and in addition, fluorescent staining was applied to visualize the morphology of osteoblasts.

#### *3.2.4.1 MTT assay*

The MTT assay was applied as described in section 3.1.5.1.

#### *3.2.4.2 AlamarBlue® assay*

AlamarBlue® (AB, G Biosciences, USA) is a non-toxic, water-soluble indicator dye, employed for the quantitative measurement of the proliferation of human and animal cells, bacteria, and fungi. Thanks to its favorable chemical and biological properties, it is suitable for real-time monitoring of cell culture viability. The dye includes an oxidation-reduction indicator (resazurin) that can undergo a color change due to chemical reduction resulting from cell growth. According to the manufacturer's recommendations, the culture medium was supplemented with 10% of AB after 24 and 72 hours and incubated for 3.5 hours [87]. The optical density was measured at 570 nm and 600 nm with a Multiscan GO spectrophotometer (ThermoFisher Scientific, USA).

#### *3.2.4.3 LDH assay*

The LDH Cytotoxicity Detection Kit (Takara Bio Inc., Japan) was employed to assess the ratio of viable and non-viable cells. LDH (lactate dehydrogenase) is a stable cytoplasmic enzyme found in abundance in nearly all cells. The release of this enzyme into the culture supernatant is directly correlated with the extent of cell damage and can be quantified through photometric measurement using a plate reader. Osteoblasts were cultured and subsequently lysed using 1% Triton X (Roth Industries, Germany) on control Ti disks, which were utilized as positive controls. Optical density readings were taken at 492 nm and 620 nm using a Multiscan GO spectrophotometer. The cytotoxicity percentage of the treated disks was calculated using a formula that incorporates the OD values of the control disks (low control) and the Triton X-treated disks (high control) [88].

#### *3.2.4.4 Visualization with fluorescent microscopy*

Primary osteoblast cells were stained with the same method as described earlier in section 3.1.5.2.

### ***3.2.5. Statistical analyses***

For contact angle measurements ($\Theta$ (°)), the means ± standard deviations (SD) were computed, and the chemical agent-treated groups were compared to the control group using an unpaired Student t-test. The means ± standard error of the mean (SE) were determined for each optical densitometry (OD) value. Subsequently, after confirming normality through testing, the data were analyzed using the nonparametric Kruskal-Wallis test in SPSS 21 software (Chicago, Illinois, USA). Statistical significance was considered at a p-value of less than 0.05.

# 4. RESULTS

## 4.1 Structural characterization and cell viability studies of photoactive nanohybrid films on Ti implant surface

### *4.1.1 SEM images of the surfaces*

Scanning electron microscopy (SEM) images (Figure 6) unveiled noticeable disparities in the surface morphology of the specimens, particularly when observed at higher magnification (×5000). The polished surface appeared predominantly flat, displaying slight scratching attributable to the polishing process. In contrast, the SA Ti disks exhibited distinctive surface attributes characterized by irregular surface features, such as grooves and valleys. The $TiO_2$ copolymer film exhibited an amorphous surface structure on the microscale, while the silver-containing polymer film showcased characteristic sub-spherical grains.

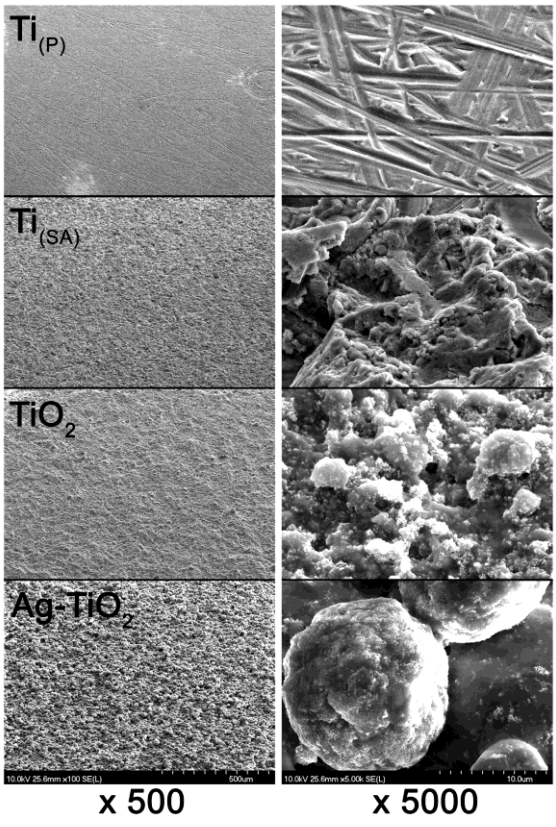


**Figure 6.** SEM images of the different surfaces without cells. Surfaces are presented in the first column at ×500 magnification (overall view) and in the second column at a higher, ×5000 magnification for better visualization.

### *4.1.2 Surface roughness measurements*

Profilometry (Figures 7 and 8) corroborated the previously mentioned disparities in surface morphology observed in the SEM images. Polished titanium exhibited the smoothest surface with a roughness value (Ra) of 0.13 µm. In contrast, both $Ti_{SA}$ and $TiO_2$ copolymer-coated disks exhibited similar roughness values ($Ti_{SA}$: Ra = 1.26 µm; $TiO_2$: Ra = 1.79 µm). Notably, the Ag-$TiO_2$ coated samples displayed significantly rougher surfaces (Ag-$TiO_2$: Ra = 5.76 µm), characterized by substantial height variations along the scanning direction.

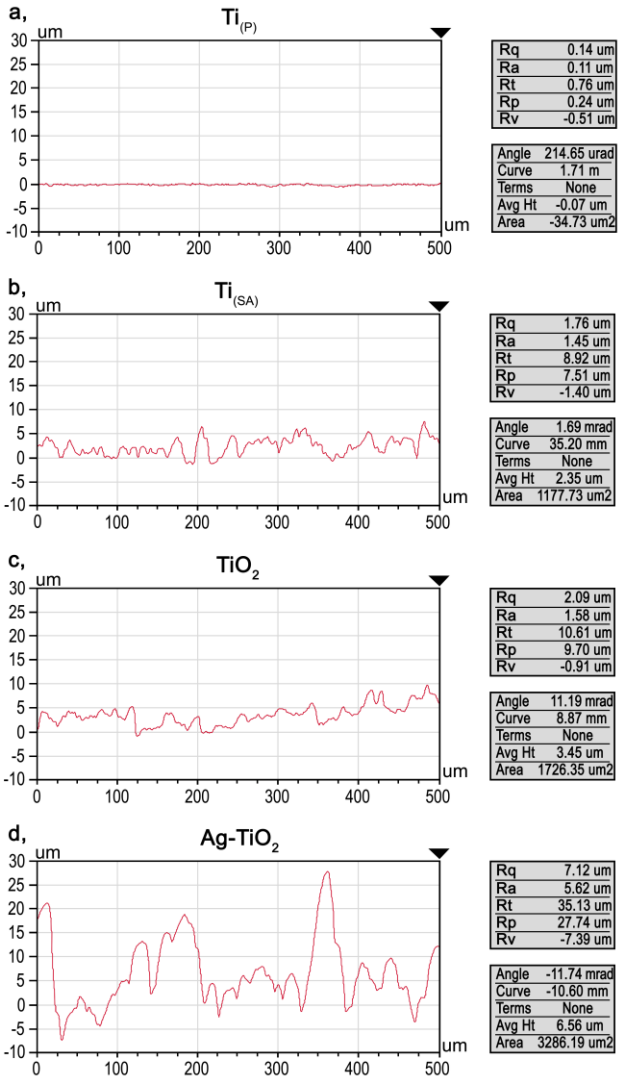


**Figure 7.** Characteristic 2D line profiles of $Ti_{(P)}$ (a); $Ti_{(SA)}$ (b); $TiO_2$ copolymer (c) and Ag-$TiO_2$ copolymer (d) coated surfaces (Ra (µm)) along a 500 µm line. Vertical height scale ranges from -10 to 30 µm.

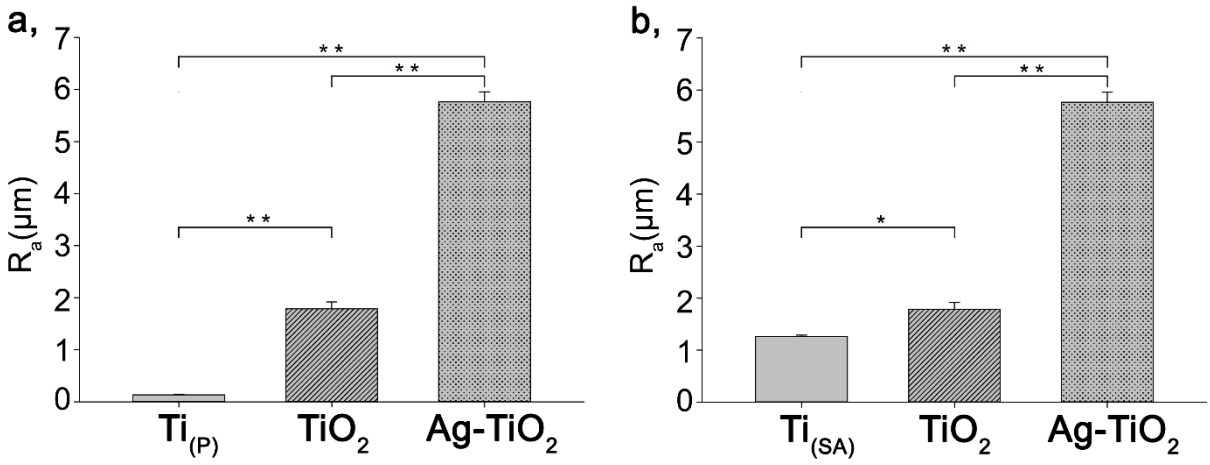


**Figure 8.** Average surface roughness values of control polished (a) and sandblasted, acid-etched Ti (b) disks compared to polymer coated samples (Ra (μm)). Data are given as mean ± SE. One-way ANOVA followed by Tukey's HSD post hoc test was utilized to determine the level of significance. Asterisks denote significant differences (* $p < 0.05$ and ** $p < 0.0001$).

### *4.1.3 MTT assay*

The bar graphs in Figure 9 display the mean ± SE of the $OD_{540nm}$ values, which are associated with cell attachment at 24 hours and cell proliferation at 72 hours and 168 hours.

In terms of cell attachment at 24 hours, there was a significant difference observed between the Ag-$TiO_2$ modified surface ($OD_{540nm,\ Ag\text{-}TiO2} = 0.08 \pm 0.004$) and the polished control Ti surface ($OD_{540nm,\ Ti\ (P)} = 0.05 \pm 0.004$), with the former showing significantly higher attachment ($p = 0.013$). The level of attachment on the Ag-$TiO_2$ surface nearly reached the values seen on the control plate, while no significant differences were found in cell attachment between the two copolymer-coated disks.

Regarding early proliferation at 72 hours, epithelial cells exhibited similar growth rates on all investigated disks ($OD_{540nm,\ Ti\ (P)} = 0.07 \pm 0.012$, $OD_{540nm,\ TiO2} = 0.06 \pm 0.002$, $OD_{540nm,\ Ag\text{-}TiO2} = 0.07 \pm 0.004$). After 168 hours, no significant differences were observed between polished Ti and either of the nanohybrid films. However, higher optical densities (ODs) were recorded on the AgNP-modified disk compared to the TiO2-polymer covered disks ($OD_{540nm,\ TiO2} = 0.05 \pm 0.001$, $OD_{540nm,\ Ag\text{-}TiO2} = 0.08 \pm 0.004$).

From another perspective, there was a significant increase ($p = 0.023$) in cell count on the polished Ti surface after one week, while at the same time point, a significant decrease ($p = 0.003$) was noted in cell count on the $TiO_2$-modified samples. Epithelial cells did not exhibit

a high proliferation rate on the Ag-$TiO_2$-coated disks, but cell growth and cell death appeared to be well balanced.

In Figure 9b, one can observe the $OD_{540}$ values representing MG-63 cell behavior on various samples. These cells exhibited a growth pattern similar to epithelial cells. At the 24-hour mark, there were no significant differences in MG-63 cell attachment between the coated surfaces and the control Ti surfaces ($OD_{540nm, Ti (SA)} = 0.06 \pm 0.005$, $OD_{540nm, TiO2} = 0.06 \pm 0.003$, $OD_{540nm, Ag\text{-}TiO2} = 0.07 \pm 0.004$). However, significantly more cells ($p = 0.03$) attached to the surface of nanosilver-coated disks compared to $TiO_2$-copolymer-coated disks.

During the early proliferation phase (72 hours), cell growth was significantly higher on the control Ti surface than on the $TiO_2$-copolymer and nanosilver-coated samples ($p < 0.001$). After 168 hours, a substantial increase in cell proliferation was observed on the uncoated Ti surfaces, whereas on the nanohybrid surfaces, the cells did not exhibit any noticeable growth tendency ($OD_{540nm, Ti (SA)} = 0.28 \pm 0.022$, $OD_{540nm, TiO2} = 0.06 \pm 0.001$, $OD_{540nm, Ag\text{-}TiO2} = 0.08 \pm 0.005$). However, there were no statistical differences observed between the copolymer-treated groups after both 72 and 168 hours.

The notable increase in cell numbers on the control Ti and untreated Ti disks underscores the viability of MG-63 cells. According to our findings, these cells did not display any signs of proliferation on the polymer-coated disks. Importantly, there were no significant differences in cell numbers among the modified samples throughout our experiments.

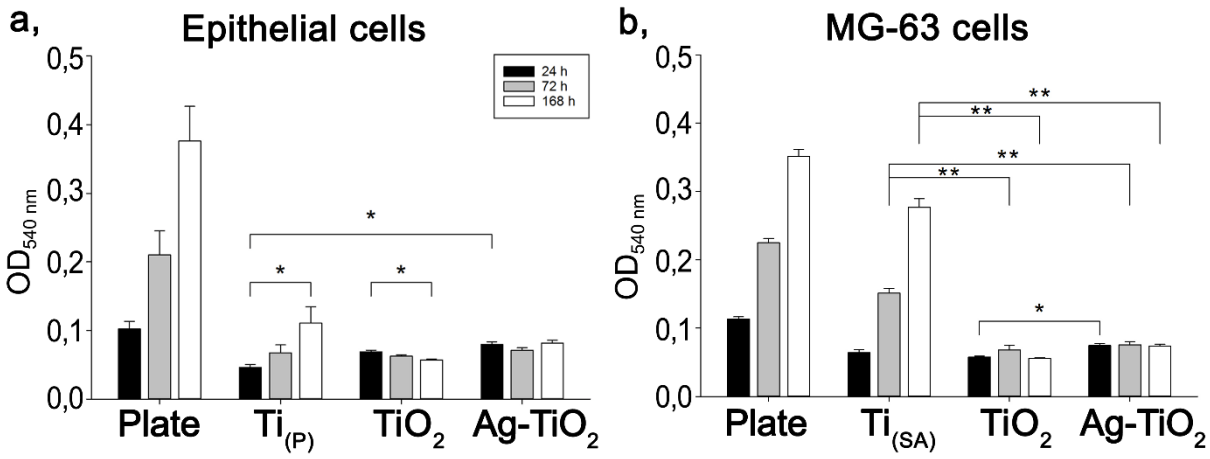


**Figure 9.** 24, 72 and 168 h $OD_{540}$ values of epithelial cells (a) and MG-63 cells (b) incubated with MTT on the control disks (plate and uncovered Ti) and on the $TiO_2$ and Ag-modified $TiO_2$ polymer covered disks. Data are presented as mean ± SE. Asterisks denote significant differences (* $p < 0.05$ and ** $p < 0.0001$).

### *4.1.4 Fluorescent images*

Composite images of epithelial and MG-63 cells were generated by merging images captured using two different filters (Figure 10). The actin cytoskeleton was represented in red (TRITC-phalloidin), while the DNA content of the cell nucleus was depicted in blue (Hoechst 33342).

In terms of epithelial cell attachment, we observed no significant differences among the three groups, but the silver-modified disks exhibited more extensive cell coverage. All three groups displayed a typical polygonal cell morphology with a few filopodia. After 72 hours, we noted increased proliferation on the polished and Ag-$TiO_2$, with cells displaying well-spread morphologies. Conversely, a decrease in proliferation was observed on the $TiO_2$ polymer-modified samples. On the Ag-$TiO_2$ samples, the cytoskeleton was not clearly visible between the grains, despite good visibility of cell nuclei. One week later, polygonal cells covered the entire surface of polished Ti disks, accompanied by several filopodia. Cell counts remained consistent on the Ag-modified surfaces, while only a few poorly spread cells were detected on the $TiO_2$-copolymer-coated disks. A notable number of rounded cells were observed on the polymer-covered disks, indicating cell detachment.

For MG-63 cell attachment, we observed similar behavior in the polymer-covered groups. Cells exhibited flat morphology with some processes and covered the surfaces in a dispersed manner without any specific orientation. The largest number of cells with rounded morphology was found on the Ag-modified surface. After 72 hours, a higher density of characteristic triangle-shaped cells was observed on the untreated Ti disks. MG-63 cells did not show any signs of proliferation on the $TiO_2$ and Ag-$TiO_2$ samples. After one week, cells covered the entire surface of the uncovered Ti disks, in contrast to the $TiO_2$ and Ag-$TiO_2$ copolymer disks, where only a few cells were present.

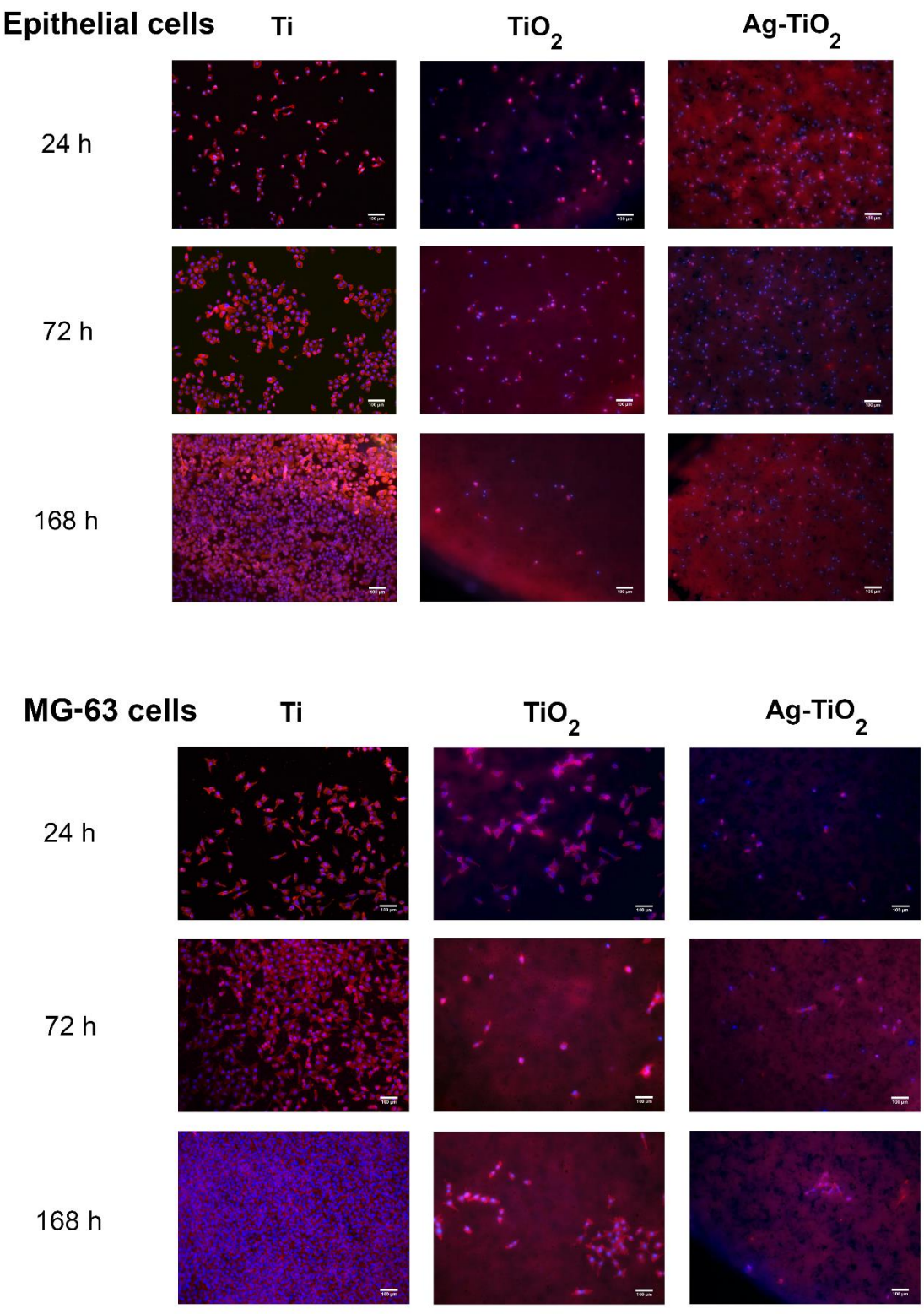


**Figure 10**. Fluorescent images of primary epithelial (a) and MG-63 cells (b) attachment and proliferation after 24 h, 72 h and 168 h by TRITC-phalloidin and Hoechst 33342 fluorescent staining: control Ti, $TiO_2$ and Ag-$TiO_2$ surfaces at a magnification of ×100. The scale bar indicates 100μm.

## 4.2 Evaluation of the effect of different chemical agents used as supportive therapy on Ti implant surfaces

### *4.2.1 Contact angle measurements*

The results of the surface wettability tests are displayed in Figure 11 and summarized in Table 1. When considering PW drops, the control titanium samples exhibited an average contact angle (θ) of 24.6 ± 5.4, with no statistically significant difference observed in the PVPI treated group (θ = 24.9 ± 4.1) in comparison to the control discs. However, both $ClO_2$ (θ = 39.2 ± 9.8) and CHX (θ = 47.2 ± 4.1) treated discs displayed significantly higher contact angle values ($p_{ClO2}$=0.012; $p_{CHX}$ < 0.0001) when compared to the control group.

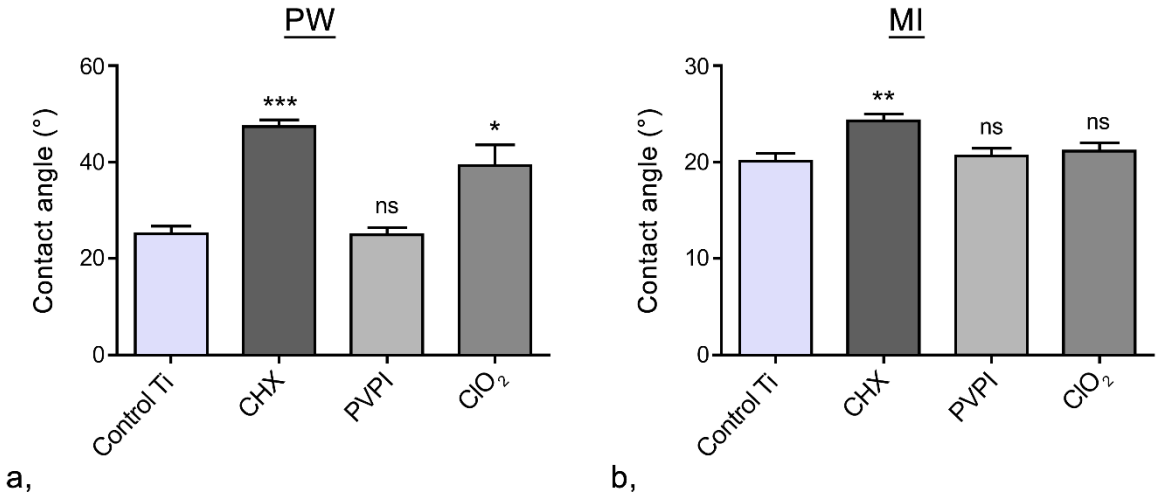


**Figure 11.** Surface wettability of the different chemical agent treated samples determined with PW (a) and MI (b) drops. Data are presented as mean ± SD. NS= not significant, asterisks denote significant differences compared to control Ti (*p <0.05, **p<0.01 and ***p < 0.001).

MI drops were used to test the samples, and the following contact angle values were recorded: $\Theta_{control\ Ti}$ = 20.1 ± 2.1; $\Theta_{PVPI}$ = 20.6 ± 2; $\Theta_{ClO2}$ = 21.1 ± 2.3; $\Theta_{CHX}$ = 24.3 ± 1.7. These measurements revealed relatively minor differences among the groups, with only the CHX treated group exhibiting a significantly higher Θ (p = 0.003) in comparison to the control.

Using the OWRK-method, the Surface Free Energy (SFE), along with it's disperse ($\gamma^d$) and polar ($\gamma^p$) components, were determined using SCA software. The results are presented in Table 1. Among the three antiseptic solutions, only the PVPI treatment was able to maintain a similar SFE ($\gamma$ = 70.7 mJ/m$^2$) to that of the control surface ($\gamma$ = 70.9 mJ/m$^2$). Significant

differences were observed in γ following CHX and $ClO_2$ treatments, resulting in γ values of 59.5 mJ/m$^2$ and 64.1 mJ/m$^2$, respectively. This led to a decrease in the polar component of the SFE, while the disperse component remained nearly unchanged.

| Surface | SFE γ (mJ/m$^2$) | $\gamma^d$ (mJ/m$^2$) | $\gamma^p$ (mJ/m$^2$) |
|---|---|---|---|
| **Control Ti** | **70.9** | **36.6** | **34.3** |
| **CHX treated** | **59.5 **** | **37.8** | **21.7** |
| **PVPI treated** | **70.7** | **36.5** | **34.2** |
| **$ClO_2$ treated** | **64.1 *** | **37.8** | **26.4** |

**Table 1.** The SFE (γ) and it's disperse ($\gamma^d$) and polar ($\gamma^p$) components of the disks, calculated with the Owen-Wendt-Rabel-Kaelble (OWRK) method. Data presented as means. Asterisks denote significant differences compared to control Ti (*p <0.05, **p<0.01 and ***p < 0.001).

### *4.2.2 XPS results*

The X-ray Photoelectron Spectroscopy (XPS) spectra, as depicted in Figure 12a, confirmed the presence of titanium (Ti), oxygen (O), and carbon (C) on both the untreated and treated titanium (Ti) samples. These elements are typically observed on the surfaces under investigation, with the positions and intensity of the O 1s and Ti 2p peaks providing evidence of an intact $TiO_2$ layer [89]. This $TiO_2$ layer is characterized by distinct peaks at 464.5 eV (Ti $2p_{1/2}$) and 458.6 eV (Ti $2p_{3/2}$). Additionally, the presence of carbonaceous contamination is indicated by the C 1s signal (peak at approximately 290 eV), which can be attributed to the adsorption of carbon-containing molecules from exposure to the surrounding air [90, 91].

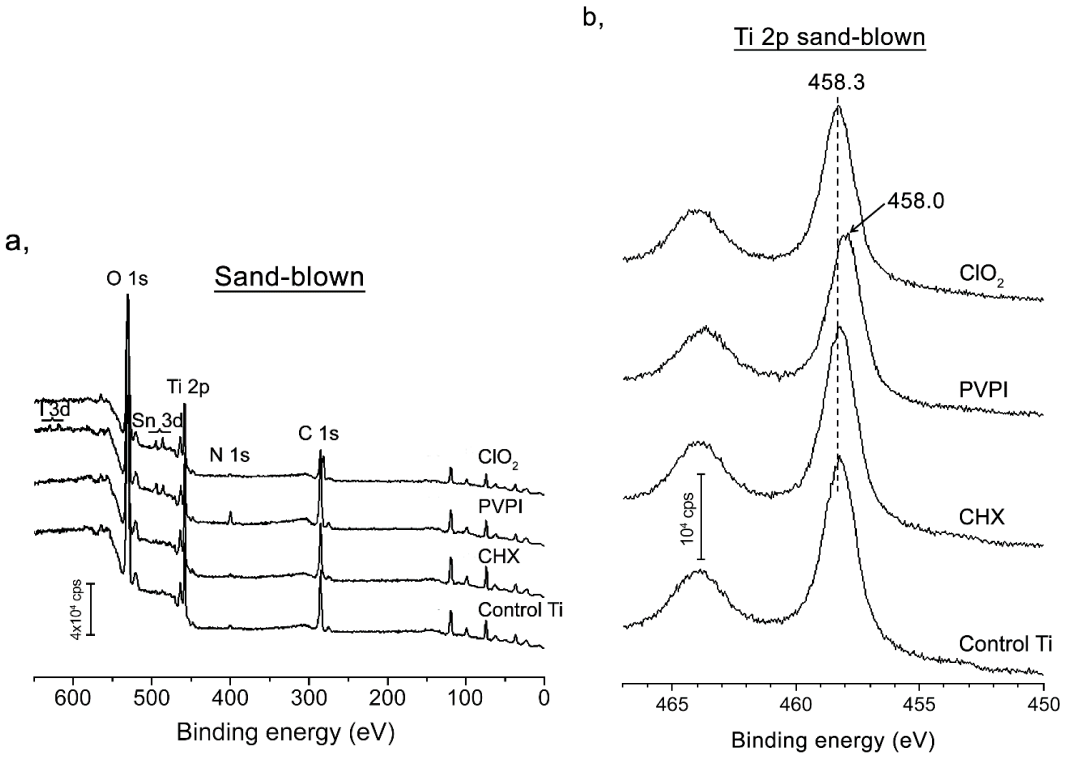


**Figure 12.** XPS spectra (a) of the control and the treated titanium disks. High-resolution XPS spectra (b) showing Ti 2p lines of untreated and treated titanium samples.

Figure 12b displays representative high-resolution Ti 2p spectra of the examined Ti samples. In these spectra, a distinctive shoulder with a peak around 462 eV is evident, which can be attributed to either a metallic form of titanium or a titanium nitride (TiN) compound. The presence of this metallic peak in the surface spectra can be attributed to the thinness of the surface oxide layer, allowing photoelectrons from the metal just beneath the metal-oxide interface to pass through the oxide layer and be detected [92]. Additionally, trace amounts of nitrogen (N) were detected in samples treated with PVPI or CHX, as indicated by peaks at approximately 453.5 eV and around 400 eV. These N peaks are a consequence of the sample fabrication process. In summary, based on the XPS spectra, it can be inferred that these chemical agents did not induce significant alterations in the surface chemistry of titanium.

### *4.2.3 MTT assay*

Figure 13 presents an overview of the outcomes from various cell viability assessments. The reduction of MTT, indicative of the number of viable osteoblast cells, is represented in the bar graph shown in Figure 13a. When examining cellular attachment (at 24 hours), it was

notably higher on the control plate ($p < 0.001$) compared to the Ti disks. However, no significant disparities were observed between the control disk and the disks treated with chemical agents ($OD_{570nm, Ti} = 0.031 \pm 0.001$, $OD_{570nm, CHX} = 0.034 \pm 0.002$, $OD_{570nm, PVPI} = 0.033 \pm 0.002$, $OD_{570nm, ClO2} = 0.032 \pm 0.001$).

Subsequent measurements taken after 72 hours indicated a high rate of proliferation on both treated and untreated Ti surfaces, with no statistically significant differences ($OD_{570nm, Ti} = 0.142 \pm 0.014$, $OD_{570nm, CHX} = 0.147 \pm 0.021$, $OD_{570nm, PVPI} = 0.136 \pm 0.017$, $OD_{570nm, ClO2} = 0.143 \pm 0.017$). Notably, all examined groups exhibited a substantial increase in cell numbers. Surprisingly, the rate of proliferation was even higher on the treated Ti disks (approximately 4.5 times) than on the control plate (approximately 3.8 times). This marked increase in proliferation rate ($p < 0.001$) underscores the viability of the primary cells under investigation. Importantly, the MTT test revealed negligible detrimental effects of the different antibacterial agents on cellular response.

### *4.2.4 AlamarBlue®*

The viability of primary Ob cells was assessed by measuring the reduction of resazurin dye. The percentage reduction of AB, represented as the mean ± SE, is displayed in the bar graphs presented in Figure 13b. There were no significant differences observed between the control and treated groups, both at 24 hours and 72 hours.

However, a significant difference ($p = 0.021$) was noted in the reduction of AB across all samples when comparing attachment and proliferation data. These findings validate the observed trend in cell growth recorded during the MTT assay.

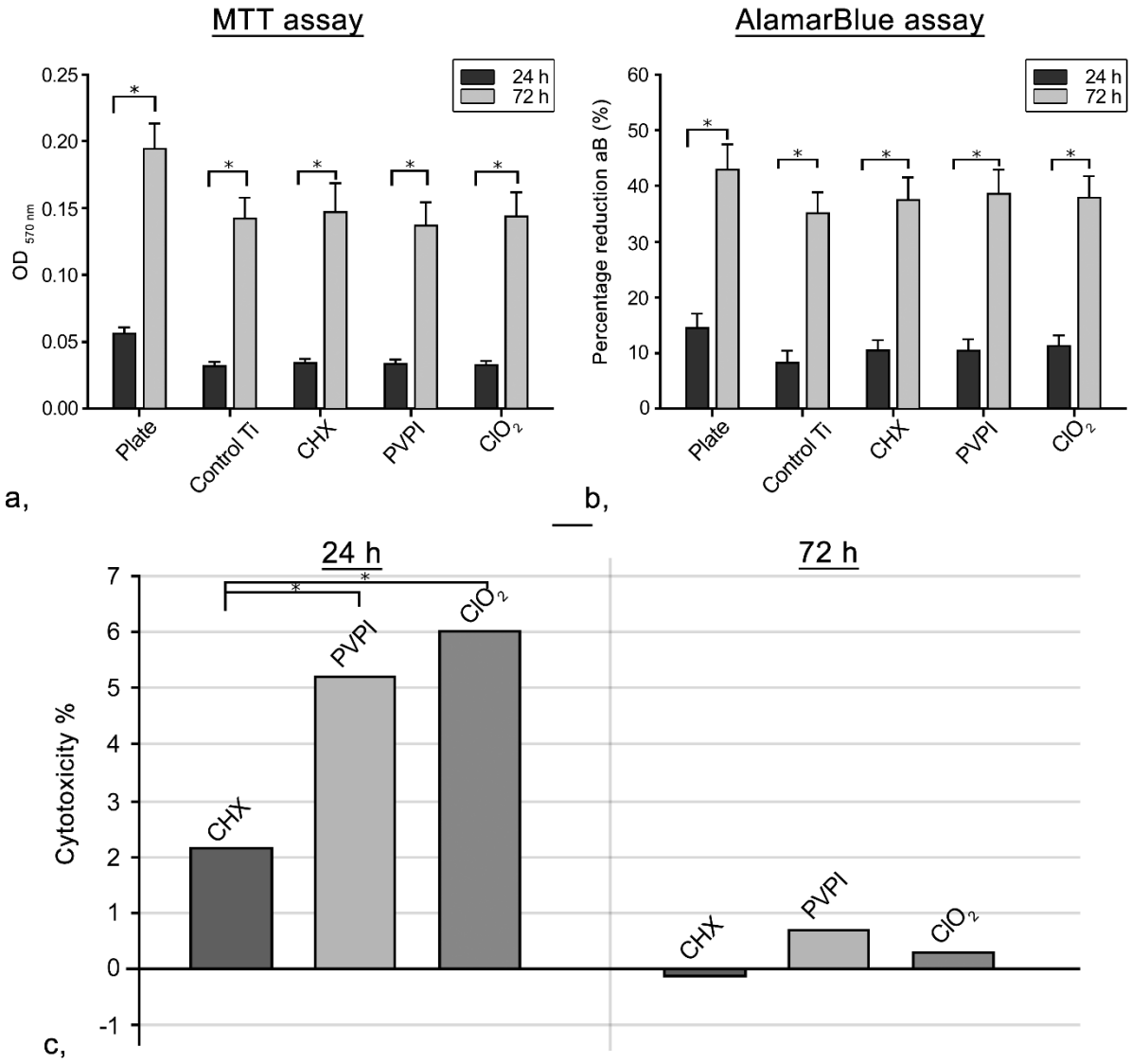


**Figure 13**. Attachment (24h) and proliferation (72h) values of osteoblast cells incubated with MTT (a) on the control (plate and uncovered Ti) and chemical agent treated disks. Data are presented as mean ± SE. Percentage reduction of alamarBlue® (b) on the control (plate and uncovered Ti) and chemical agent treated disks. Data are presented as mean % ± SE. Cytotoxicity was measured by the release of lactate-dehydrogenase from the cultivated osteoblast cells (c). The bar graphs illustrate the % difference in cell death of the treated disks compared to the control disks. Data are presented as mean %. Asterisks denote significant differences ($*p < 0.05$).

### *4.2.5 LDH assay*

In addition to the two cell viability assessments, a standard cytotoxicity study was conducted. The cytotoxicity percentages of the samples are depicted in the bar graph presented in Figure 13c. After 24 hours, it was observed that the CHX treated group (2%) exhibited the

lowest cytotoxicity compared to the other two groups (more than 5%). There was no significant difference in the number of damaged cells in the treated Ti samples (approximately 0% cytotoxicity) after 72 hours compared to the control group. The minimal release of LDH in the treated groups indicates that the titanium surfaces remained highly compatible with cell viability after a 5-minute treatment with the antibacterial solutions.

### *4.2.6 Visualization with fluorescent microscopy*

Fluorescent images of primary osteoblast (Ob) cells are displayed in Figure 14. The actin cytoskeleton of the cells is visualized in red (TRITC-phalloidin), and the cell nucleus is stained blue (Hoechst 33342). Similar cellular attachment patterns were consistently observed, characterized by the typical polygonal morphology of osteoblast cells with some filopodia, across all investigated groups. After 72 hours, a significant increase in cell proliferation was evident in each group, with cells densely covering the surfaces. In certain areas of the disks, multiple layers of cells were observed. This suggests that the cells found the disks conducive for cell division.

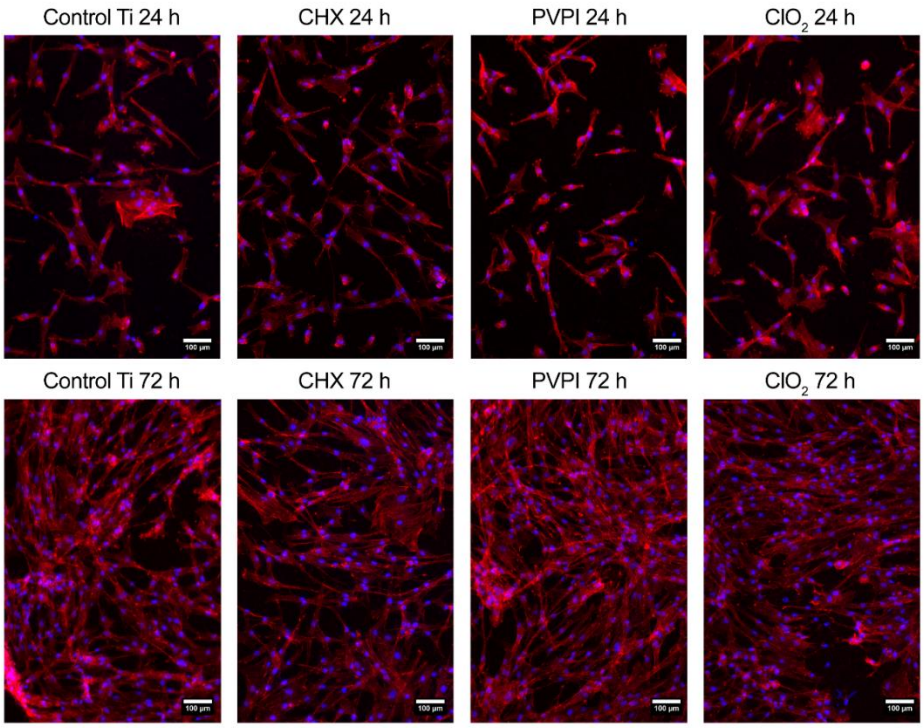


**Figure 14.** Fluorescent images of primary osteoblast cells attachment and proliferation after 24h and 72h at a magnification of ×100.

# 5. DISCUSSION

Two primary trends are driving research in the field of dental implant surface modifications. One is to enhance biocompatibility (accelerate osseointegration), and the other is to bolster bacterial resistance. Improving the antibacterial properties of dental implants has garnered significant scientific interest in recent years [22]. Nevertheless, these aspects are deeply interconnected because an excellent antibacterial surface can only be applied if its biocompatibility remains unaltered or at least acceptable for human cells to proliferate. My doctoral work primarily focuses on the antimicrobial aspect, further investigating two different strategies in the fight against bacteria: photo-activated nanohybrid coatings (for prevention and therapy) and the interaction of oral antiseptics (for therapy) with a Ti model surface. While antibacterial properties have been well described by other members of our research group, my goal was to examine the cellular response of various primary cells and cell lines to modified Ti surfaces.

## 5.1 Biocompatibility and surface characterization of the nanocomposite films

The first part of my thesis focuses on conducting a biocompatibility study involving two newly developed nanohybrid coatings: $TiO_2$-copolymer and $AgTiO_2$-copolymer films. Following structural characterization, basic cell culture viability tests were performed with MG-63 osteosarcoma and mucosa derived epithelial cells. The incorporation of various noble metal nanoparticles into $TiO_2$ photocatalytic polymer films has been a widely adopted approach to extend light absorption from the UV to visible range. The introduction of silver into these films not only imparts photocatalytic activity but also antibacterial properties. Tallósy et al. verified the surface accumulation of the Ag-$TiO_2$ photocatalyst on the film surfaces, with concurrent partial degradation of polymer chains. This unique property enables direct interaction between bacteria and cells with the nanoparticles [54]. These nanohybrid films hold potential for applications as thin coatings on the neck part of implants, primarily aimed at preventing or even treating peri-implant infections.

Two-dimensional height differences (Ra) were recorded using a profilometer. Smooth titanium (Ti) served as the control for epithelial cells, whereas sandblasted-acid etched titanium ($Ti_{SA}$) and titanium dioxide ($TiO_2$) copolymer disks exhibited moderately rough surfaces, which are considered favorable for osteoblasts according to the research conducted by Wennerberg et

al. [93]. On the other hand, silver nanoparticles (AgNPs) resulted in the formation of large surface grains following spray coating, leading to significantly higher Ra values. Regarding the correlation between surface roughness and biocompatibility, there is controversy in *in vitro* studies reported in the literature. Nevertheless, it is widely accepted that epithelial cells tend to thrive on smooth, polished surfaces, while osteoblasts require surface irregularities to enhance osseointegration [16]. Györgyey et al. found that substantial alterations in the Ra of laser-ablated titanium disks compared to $Ti_{SA}$ disks did not result in differences in the attachment and proliferation of MG-63 cells [94]. Most *in vitro* studies have concluded that MG-63 cells exhibit a preference for rougher surfaces (with Ra values around 4-5 μm) [19]. Interestingly, despite the Ra of AgNP-modified disks being close to the ideal range, MG-63 cells displayed a notably low proliferation rate. Similarly surprising was the relatively high attachment and survival of epithelial cells on the rougher Ag-copolymer modified surface. This unexpected response of the cells may be attributed to the chemistry of the polymer matrix or the presence of nanoparticles, and further molecular research is needed to elucidate the specific sensitivity of osteosarcoma cells in this context.

Controlled, randomized clinical studies have been conducted to compare the long-term survival of machined and rough implant surfaces. These studies emphasize the importance of considering factors beyond micro-topography in assessing implant performance [95].

Our cell viability assessments were conducted using the MTT test, a commonly employed proliferation assay occasionally utilized as a cytotoxicity test based on mitochondrial activity. In contrast to findings in the existing literature, our results revealed a decrease in the quantity of epithelial cells and a low, albeit fluctuating, quantity of MG-63 cells on the $TiO_2$-copolymer modified disks. Numerous studies have affirmed the biocompatibility of titanium dioxide nanoparticles ($TiO_2$NPs). Among the various forms of $TiO_2$NPs examined, titanium nanotubes (TNT) and nanopores have been extensively investigated, showcasing excellent osseointegration properties and the potential for therapeutic release [96]. Ivask et al. reported favorable responses from epithelial and fibroblast cell lines to $TiO_2$ nanoparticles, among others, such as $Al_2O_3$, $Fe_3O_4$, MgO, $SiO_2$, and $WO_3$ [97]. A comprehensive cytotoxicity study using the MTT assay was conducted by Jeng et al., concluding that $TiO_2$ nanoparticles were well-tolerated by Neuro-2A cells at concentrations of up to 200 μg/mL [98]. Recent publications have also demonstrated high proliferation rates of primary human gingival fibroblast cells on nanoporous $TiO_2$ coatings [99]. *In vivo* research by Azzawi et al. further affirmed the significant role of nano $TiO_2$ in accelerating osseointegration in rabbit tibia [100].

The variation in epithelial cell proliferation observed in our study could potentially be attributed to size-dependent toxicity of $TiO_2$NPs [41], because smaller particles are more readily taken up and internalized by cells. Additionally, the specific sensitivity of cells to the polymer matrix (p(EA-co-MMA)) or the potential release of polyacrylate from the coatings may provide further explanations.

Epithelial cells primarily interact with the polymer-coated titanium, typically found in the neck portion of the implant or abutment. Achieving a seamless gingival closure is crucial to prevent bacterial infiltration into deeper tissues and to mitigate the risk of peri-implantitis. Our MTT tests revealed that the attachment of gingival epithelial cells to the Ag-$TiO_2$-copolymer-coated disks was significantly higher when compared to the polished Ti control samples. Despite this promising attachment, these epithelial cells did not exhibit a significant growth trend on the AgNP-coated samples, and the relative cell mass remained stable throughout the duration of the study.

Several researchers have explored the *in vitro* responses of epithelial cells to dental implants with nanoscale modifications. In line with our findings, Mei et al. demonstrated robust epithelial cell viability and proliferation on Ti dental implants embedded with silver (Ag) and $TiO_2$ nanotubes [101]. Additionally, an *in vivo* study by Rossi et al. reported enhanced epithelial attachment on nanoporous sol-gel-derived $TiO_2$ surface-treated implants in comparison to untreated control implants [102].

Nanohybrid coatings also have the potential to interact with the alveolar bone, particularly in the case of implants placed at deeper levels or in the context of guided bone regeneration (GBR). To assess the response of osteoblast cells, we employed the most commonly used immortalized cell line, as the separation of primary osteoblast cells had not yet been completed at the time of this study. MG-63 cells faced challenges in terms of survival on the photocatalytic films, with stagnant or even declining cell numbers observed. However, living cells were detected on both polymer coatings after one week of incubation, suggesting the possibility of delayed proliferation. Other researchers have also investigated the reduced viability of immortalized cell lines on surfaces incorporating silver nanoparticles (AgNPs). De Giglio et al. developed hydrogel thin films based on polyacrylate coupled with AgNPs on titanium implant materials used in orthopedics and dentistry. They achieved long-term antibacterial activity through controlled release of $Ag^+$ ions. In accordance with our findings, they observed a decrease in MG-63 cell viability during the initial days of incubation, but after one week, cell proliferation increased [103]. Moaddab and colleagues determined the cytotoxic

threshold of nanosilver for the osteoblast cell line G292, noting that the inhibition of proliferation was concentration-dependent, with an IC50 value of 3.42 μg/mL [104]. In recent years, the use of silver nanoparticles for cancer therapy has gained significant attention. Cancer cells have been found to be more susceptible to nanosilver than normal human cells. Numerous authors have published studies on the cytotoxicity of AgNPs against various types of cancer cells, including hepatocellular carcinoma, adenocarcinoma, and osteosarcoma. The potential application of AgNPs in the field of anti-cancer therapies warrants further investigation through clinical studies [105, 106].

Tallósy et al. [54] provided evidence for the long-term mechanical stability of the nanohybrid films. They found that silver nanoparticles exhibited strong adhesion to the polymer matrix, with only 1.4% dissolution observed after one week of exposure to distilled water. This minimal release of AgNPs and $Ag^+$ ions may contribute to improved biocompatibility. However, contrasting conclusions regarding the biocompatibility of nanosilver-coated titanium have been reported in *in vitro* studies by other authors. Ferraris et al. explored a novel bioactive surface featuring securely attached silver nanoparticles. They assessed the viability of MG-63 osteoblast-like cells on CP Ti and Ti6Al4V samples using the MTT assay. These nanostructured surfaces exhibited favorable antibacterial properties against *S.aureus* and good cell viability on CP Ti when loaded with a low concentration of silver (0.001 M). In contrast, Ti6Al4V surfaces displayed greater cytotoxicity despite having equivalent silver content [107]. Necula et al. investigated the cytocompatibility of Ag-bearing $TiO_2$ coatings on Ti6Al7Nb alloy disks prepared using the plasma electrolytic oxidation (PEO) technique. Positive results have been reported in terms of the robust proliferation of immortalized human fetal osteoblast cells (SV-HFO) on coatings containing 0.3g/L of silver (Ag), along with demonstrated antibacterial activity against MRSA (Methicillin-resistant Staphylococcus aureus) [108]. Another research group examined the viability of MC3T3-E1 preosteoblast cells and the adhesion of bacteria on nanocoatings with minimal silver loading ($0.65 \pm 0.15$ nmol $cm^{-2}$). They observed that these monolayers significantly hindered the adhesion of both *E. coli* and *S. epidermidis*, while maintaining the viability of MC3T3-E1 cells [109]. Clinical studies involving silver nanoparticles (AgNPs) in conjunction with titanium dental implant surfaces remain limited, with the majority still in the pre-clinical phase. However, recent studies have shown promise in this regard. Salaie et al. developed hybrid surfaces on Ti6Al4V, featuring an inner layer of AgNPs responsible for antimicrobial effects and an outer layer composed of nano- and micro-scale hydroxyapatite (HA), creating an attractive interface for osteoblast cells. Despite a higher

release of silver into the cell culture medium compared to Ag-coated titanium, the viability of primary human osteoblast cells on Ag + nanoHA surfaces reached approximately 70% after one week of incubation [110]. *In vivo* studies by Smeets et al. involved silver-doped polysiloxane coatings on $Ti_{SA}$ implants in pig models. The Ag content of these coatings was approximately 1.5 $\mu g/cm^2$. While satisfactory osseointegration was observed, the bone-to-implant contact (BIC) was somewhat lower compared to the control group. Nonetheless, they confirmed the biocompatibility of AgNP-doped polymer coatings [111].

These surfaces with reduced silver content demonstrated both acceptable biocompatibility and antibacterial activity simultaneously. Achieving such a balance would be desirable for various cell types in the future, promoting the safe and long-term utilization of nanomaterials in biomedical devices.

### 5.2 Chemical agents as part of the supplementary therapy of peri-implant infections

Diseases associated with oral pathogens are prevalent global concerns, despite the availability of advanced education and patient motivation. Dental professionals face daily challenges in treating moderate to severe peri-implant infections. Antimicrobial oral solutions serve as widely employed adjunctive tools for both conservative and surgical interventions in cases of mucositis and peri-implantitis. The second part of my thesis centers on gaining a deeper understanding of the interactions between three distinct disinfectants and titanium models. This involved conducting studies on surface wettability and analyzing the elemental composition, followed by assessing the cellular viability of primary osteoblasts on titanium disks treated with chemical agents.

Surface wettability and surface free energy (SFE) are pivotal factors influencing cellular responses. In general, hydrophilic surfaces facilitate cell adhesion and exhibit lower affinity for proteins, whereas hydrophobic surfaces exhibit the opposite behavior [112]. The contact angle measurements of PVPI-treated samples closely resembled those of the control $Ti_{SA}$, while the contact angles of CHX and $ClO_2$- treated samples were similarly high. Notably, only the PVPI-treated samples were able to maintain the initial SFE of untreated titanium, suggesting the absence of any irreversible interaction between Betadine (PVPI) and titanium. Despite statistically significant differences in the wettability of the antibacterial agent-treated disks, all samples remained within the hydrophilic range ($\Theta < 90^o$). These findings align with those reported by Kubies et al., who emphasized the relatively minor role of contact angle and surface

free energy in the proliferation of normal human osteoblast cells on various titanium and non-metallic materials, with surface roughness being of greater importance [83]. Another study demonstrated that MG-63 cells exhibited greater attachment to titanium (Ti) surfaces that were subjected to $Al_2O_3$ blasting and sandblasting followed by acid etching. These surfaces had lower contact angles, indicating higher hydrophilicity, in comparison to polished and etched Ti surfaces. However, when assessing cell proliferation after 48 hours, it was observed that the etched Ti surfaces outperformed the blasted ones [113]. Abusahba et al. investigated the impact of various air-abrasive treatments on sandblasted and acid etched Ti surfaces. They found that the air-abraded surfaces exhibited higher surface free energy and wettability, leading to increased proliferation of MC3T3-E1 cells in comparison to non-abraded control surfaces [114]. These studies collectively underline the positive influence of enhanced wettability on cellular responses. Nevertheless, they also underscore the significance of other surface characteristics such as roughness, chemical composition, and the presence of residual elements.

The metabolic activity of osteoblasts on the treated samples was assessed using various bioassays, including MTT, AB, and a cytotoxicity study employing LDH. Interestingly, there was no significant difference observed in the proliferation rate of osteoblast cells across the treated samples. The sole notable change was a higher number of damaged cells at the 24-hour mark, with CHX-treated samples appearing to exhibit greater cytocompatibility. Despite the anticipated substantial shift in surface free energy (SFE), which was expected to be a critical factor influencing biological responses, primary osteoblast cells demonstrated tolerance towards the higher contact angle ($\Theta$) and lower SFE associated with CHX and $ClO_2$-treated disks.

Chlorhexidine (CHX), widely regarded as the gold standard antiseptic in periodontology, has been found to be less compatible with bone cells. A recent *in vitro* study reported reduced proliferation and an increased presence of apoptotic primary osteoblast cells after one-minute exposure to 0.12% and 0.2% CHX solutions [115]. Similarly, Almazin et al. identified 0.5 mg/ml CHX solution as cytotoxic to primary osteoblasts [116]. Notably, these studies differed in experimental conditions compared to our research. They examined the direct contact effect of undiluted CHX solutions on osteoblast cells, whereas our study assessed the response of osteoblasts on Ti surfaces treated with CHX for five minutes and subsequently rinsed three times with water. This extensive dilution of the antibacterial solutions likely resulted in only trace amounts of the agents remaining on the surfaces. The thorough three-time rinse in ultrapure water proved effective in removing antiseptics, as evidenced by the detection

of only the typical elements of CP4 Ti implant surfaces through XPS analysis. Kozlovsky et al. evaluated the substantivity of CHX on both smooth and rough Ti surfaces, discovering higher levels of released CHX and greater bacterial inhibition on rougher Ti surfaces when exposed to 0.2% CHX aqueous solutions [117]. Earlier, other members of our research group also confirmed the presence of CHX remnants on CP4 Ti surfaces. However, their investigation focused on polished Ti disks and employed a more concentrated (1% w/w) CHX gel [15]. It appears that surface roughness and the concentration of the chemical agent are pivotal factors influencing adsorption onto titanium surfaces.

The antibacterial effectiveness of these solutions has been previously confirmed by numerous authors [118-120]. In alignment with our research, a study conducted by Venkei et al. investigated the antibacterial properties of the three chemical disinfectants: chlorhexidine (CHX), povidone-iodine (PVPI), and chlorine dioxide ($ClO_2$). They highlighted the superior performance of PVPI and $ClO_2$ in eradicating pioneer colonizing bacteria such as *S. mitis* and *S. salivarius*, in comparison to CHX [121]. Barrak et al. also observed that PVPI exhibited greater efficacy in reducing the number of *P. gingivalis* on titanium samples when compared to CHX [122].

A limited number of publications exist concerning the biocompatibility of titanium biomaterials treated with povidone-iodine (PVPI) or chlorine dioxide ($ClO_2$). In a clinical study conducted by Kabata et al., povidone-iodine-coated titanium hip prostheses were evaluated, and no signs of cytotoxicity were reported during an average follow-up period of 33 months [123]. Similarly, Ma et al. concluded that lower concentrations (below 200 ppm) of chlorine dioxide solutions exhibited cytocompatibility [124]. Nevertheless, as of recent times, no studies have been published that investigate cellular responses to titanium surfaces following chlorine dioxide treatment. The significance of this study stems from the fact that primary osteoblasts displayed robust viability on these treated surfaces. In the treatment of severe peri-implant infections, various cell types may be exposed to these chemical agents as supplemental therapy alongside mechanical debridement. The biocompatibility of treated surfaces with epithelial and fibroblast cells is crucial for achieving a seamless gingival closure around the implant, particularly in cases of guided bone regeneration (GBR) or regenerative therapy for peri-implantitis. In such scenarios, which may involve possible re-osseointegration, osteoblasts could also come into contact with the previously contaminated titanium surface.

As antimicrobial resistance becomes increasingly prevalent, the demand for potent antibacterial enhancements of titanium surfaces and chemical disinfectants continues to grow.

Visible light-induced Ag-$TiO_2$ nanohybrid coatings have elicited promising responses from host cells, along with high bacterial toxicity. When used as supplemental therapy, solutions based on povidone-iodine (PVPI) and/or chlorine dioxide ($ClO_2$) have the potential to further reduce bacterial loads to non-pathogenic levels, thereby sustaining inflammation-free conditions over extended periods. To gain a deeper understanding of the response of the alveolar bone and gingival tissues as a complex system to these coatings and chemical antiseptics, further *in vivo* and clinical trials are essential.

# 6. SUMMARY AND CONCLUSIONS

Biomaterials offer a unique opportunity to restore impaired functions of the human musculoskeletal system. Among the most extensively researched biomaterials in healthcare, titanium dental implants have been a focal point of both industrial and dental research for decades. Bacterial adhesion to implant surfaces, either alone or in combination with excessive loads on implant-supported prostheses, can lead to severe peri-implant infections, ultimately resulting in implant failure.

The absence of a standardized, effective treatment protocol underscores the significance of any progress made in the prevention or treatment of implant-associated infections. The primary objective of my doctoral research was to investigate the biocompatibility of titanium surfaces treated with two nanoparticle-doped polymer films and three chemical disinfectants. This investigation encompassed the examination of various physicochemical properties, including roughness, wettability, and chemical composition, alongside *in vitro* cytocompatibility tests involving a range of cell types, such as MG-63 osteosarcoma cells, primary epithelial cells, and osteoblasts.

The main conclusions of the thesis are:

1. $TiO_2$-nanohybrid films exhibited similar roughness to the control Ti, whereas $AgTiO_2$-copolymer films displayed a significant increase in Ra.
2. The newly developed photocatalytic nanohybrid coatings demonstrated excellent attachment of human epithelial cells.
3. Despite the reduced Ag content (0.001%) of the polymer coating, suppressed proliferation of MG-63 cells was observed.
4. Treatment of Ti surfaces with PVPI maintained the wettability and surface free energy (SFE) at levels comparable to untreated Ti.
5. CHX and $ClO_2$ solutions led to higher contact angles and lower SFE compared to the control, although this shift still fell within the hydrophilic range.
6. Despite the significant alterations in wettability, primary osteoblast cells exhibited a high proliferation rate on all of the surfaces.

## 7. ACKNOWLEDGEMENTS

I would like to express my deepest gratitude to my supervisors, Dr. Kinga Turzó and Dr. Krisztina Ungvári, who continuously encouraged and supported me during my scientific years. I am extremely grateful for their motivation, advices and belief in me. I am especially grateful to Dr. Gábor Braunitzer for his significant contribution to present form of the thesis and his help in statistical evaluations and lecturing scientific grammar. I am deeply indebted to Dr. Ágnes Györgyey for showing me the passion and basics of dental research and *in vitro* cell culture techniques. I am grateful to Prof Dr. János Minárovits and Dr. István Pelsőczi-Kovács who always provided the best of their knowledge to help me in scientific questions.

I would like to thank the support and help of all of my previous colleagues (Dr. Zsolt Tóth, Dr. Annamária Venkei, Dr. Anett Nagy-Demcsák, Sándor Mészáros, Dr. Henrietta Guti Pelsőczi-Kovácsné, Mária Horváth, Zsófia Papp) at the Department of Oral Biology and Experimental Dental Research. I would like to extend my sincere thanks to all of our collaborating partners and researchers from other departments of the University of Szeged. I am also thankful to Zsuzsanna Kiss-Dózsai for her help with the final illustration of my work. I would like to thank Prof. Dr. Zoltán Baráth, the dean of the Faculty of Dentistry, University of Szeged for his support to finish my doctoral work. I am also grateful to Denti System® Hungary for providing the titanium samples and the Department of Oral Surgery (Faculty of Dentistry, University of Szeged) for providing the bone chips and the gingival tissues.

Last but not least I would like to express my warmest gratitude to my fiancée Dr. Fruzsina Szeszták, my biggest bolsterer and my family for their encouragement and emotional support through my scientific years.

## 8. FINANCIAL SUPPORT

This work was supported by the grant GINOP-2.3.2-15-2016-00011 to a consortium led by the University of Szeged, Szeged, Hungary (participants: University of Debrecen, Debrecen, and the Biological Research Centre, Hungarian Academy of Sciences, Szeged, Hungary), project leader János Minárovits. The grant was funded by the European Regional Development Fund of the European Union and managed in the framework of the Economic Development and Innovation Operational Programe by the Ministry of National Economy, National Research, Development and Innovation Office, Budapest, Hungary. The research was also supported by the project entitled "ÁOK-TANDEM_palyazat_2019_09_16_ Turzó Kinga" and "ÁOK-TANDEM_palyazat_2023_04_04_Turzó Kinga" sustained by the University of Pécs, Medical Faculty.

## 9. REFERENCES


[1] Kanasi E, Ayilavarapu S, Jones J. The aging population: demographics and the biology of aging. *Periodontol 2000*. 2016;72:13-8.

[2] Williams DF. Implants in dental and maxillofacial surgery. *Biomaterials.* 1981;2:133-46.

[3] Lemons JE. Dental implant biomaterials. *Journal of the American Dental Association*. 1990;121:716-9.

[4] Brånemark PI. Osseointegration and its experimental background. *J Prosthet Dent*. 1983;50:399-410.

[5] Wang RR, Fenton A. Titanium for prosthodontic applications: a review of the literature. *Quintessence International*.1996;27:401-8.

[6] Lautenschlager EP, Monaghan P. Titanium and titanium alloys as dental materials. *International Dental Journal*. 1993;43:245-53.

[7] Tschernitschek H, Borchers L, Geurtsen W. Nonalloyed titanium as a bioinert metal-a review. *Quintessence Int.* 2005;36:523-30.

[8] Hanawa T. A comprehensive review of techniques for biofunctionalization of titanium. *J Periodontal Implant Sci.* 2011;41:263-72.

[9] Adrian P. Mouritz. Titanium alloys for aerospace structures and engines. In: Mouritz AP, editor of book. Introduction to Aerospace Materials: *Woodhead Publishing*; 2012. p. 202-23.

[10] Sarraf M, Rezvani Ghomi E, Alipour S, Ramakrishna S, Liana Sukiman N. A state-of-the-art review of the fabrication and characteristics of titanium and its alloys for biomedical applications. *Biodes Manuf.* 2022;5:371-95.

[11] Puleo DA, Nanci A. Understanding and controlling the bone-implant interface. *Biomaterials*. 1999;20:2311-21.

[12] Thompson GJ, Puleo DA. Effects of sublethal metal ion concentrations on osteogenic cells derived from bone marrow stromal cells. *J Appl Biomater*. 1995;6:249-58.

[13] Davies J. Mechanisms of Endosseous Integration. *The International journal of prosthodontics.* 1998;11:391-401.

[14] Ivanovski S, Lee R. Comparison of peri-implant and periodontal marginal soft tissues in health and disease. *Periodontol 2000*. 2018;76:116-30.

[15] Ungvári K, Pelsöczi IK, Kormos B, Oszkó A, Rakonczay Z, Kemény L, et al. Effects on titanium implant surfaces of chemical agents used for the treatment of peri-implantitis. *Journal of Biomedical Materials Research Part B, Applied Biomaterials.* 2010;94:222-9.

[16] Turzo K. Surface Aspects of Titanium Dental Implants. In: Reda Helmy S, editor. Biotechnology. Rijeka: *IntechOpen;* 2012. p. Ch. 9.

[17] Klinge B, Meyle J, Working G. Soft-tissue integration of implants. Consensus report of Working Group 2. *Clinical Oral Implants Research*. 2006;17 Suppl 2:93-6.

[18] Czekanska EM, Stoddart MJ, Richards RG, Hayes JS. In search of an osteoblast cell model for in vitro research. *Eur Cell Mater*. 2012;24:1-17.

[19] Bächle M, Kohal RJ. A systematic review of the influence of different titanium surfaces on proliferation, differentiation and protein synthesis of osteoblast-like MG63 cells. *Clinical Oral Implants Research.* 2004;15:683-92.

[20] Clover J, Gowen M. Are MG-63 and HOS TE85 human osteosarcoma cell lines representative models of the osteoblastic phenotype? *Bone*. 1994;15:585-91.

[21] Pellegrini G, Francetti L, Barbaro B, Del Fabbro M. Novel surfaces and osseointegration in implant dentistry. *J Investig Clin Dent.* 2018;9:e12349.

[22] Chouirfa H, Bouloussa H, Migonney V, Falentin-Daudré C. Review of titanium surface modification techniques and coatings for antibacterial applications. *Acta Biomater.* 2019;83:37-54.

[23] Jurak M, Wiącek AE, Ładniak A, Przykaza K, Szafran K. What affects the biocompatibility of polymers? *Advances in Colloid and Interface Science.* 2021;294:102451.

[24] Jemat A, Ghazali MJ, Razali M, Otsuka Y. Surface Modifications and Their Effects on Titanium Dental Implants. *Biomed Res Int.* 2015;791725.

[25] Zhang J, Liu J, Wang C, Chen F, Wang X, Lin K. A comparative study of the osteogenic performance between the hierarchical micro/submicro-textured 3D-printed Ti6Al4V surface and the SLA surface. *Bioact Mater*. 2020;5:9-16.

[26] Chrcanovic BR, Albrektsson T, Wennerberg A. Reasons for failures of oral implants. *J Oral Rehabil*. 2014;41:443-76.

[27] Mombelli A, Décaillet F. The characteristics of biofilms in peri-implant disease. *J Clin Periodontol.* 2011;38 Suppl 11:203-13.

[28] Heitz-Mayfield LJA, Salvi GE. Peri-implant mucositis. *J Clin Periodontol*. 2018;45 Suppl 20:S237-s45.

[29] Figuero E, Graziani F, Sanz I, Herrera D, Sanz M. Management of peri-implant mucositis and peri-implantitis. *Periodontol 2000*. 2014;66:255-73.

[30] Smeets R, Henningsen A, Jung O, Heiland M, Hammächer C, Stein JM. Definition, etiology, prevention and treatment of peri-implantitis – a review. *Head & Face Medicine*. 2014;10:34.

[31] Mombelli A, Lang NP. The diagnosis and treatment of peri-implantitis. *Periodontol 2000*. 1998;17:63-76.

[32] Klinge B, Klinge A, Bertl K, Stavropoulos A. Peri-implant diseases. *Eur J Oral Sci*. 2018;126 Suppl 1:88-94.

[33] Derks J, Tomasi C. Peri-implant health and disease. A systematic review of current epidemiology. *Journal of Clinical Periodontology*. 2015;42:S158-S71.

[34] Lee CT, Huang YW, Zhu L, Weltman R. Prevalences of peri-implantitis and peri-implant mucositis: systematic review and meta-analysis. *Journal of dentistry*. 2017;62:1-12.

[35] Yeo I-S. Reality of dental implant surface modification: a short literature review. *The Open Biomedical Engineering Journal*. 2014;8:114-9.

[36] Souza JCM, Sordi MB, Kanazawa M, Ravindran S, Henriques B, Silva FS, et al. Nano-scale modification of titanium implant surfaces to enhance osseointegration. *Acta Biomater*. 2019;94:112-31.

[37] Iesalnieks M, Eglītis R, Juhna T, Šmits K, Šutka A. Photocatalytic Activity of $TiO_{(2)}$ Coatings Obtained at Room Temperature on a Polymethyl Methacrylate Substrate. *Int J Mol Sci*. 2022;23.

[38] Allen NS, Edge M, Sandoval G, Verran J, Stratton J, Maltby J. Photocatalytic coatings for environmental applications. *Photochem Photobiol*. 2005;81:279-90.

[39] Wong MS, Chu WC, Sun DS, Huang HS, Chen JH, Tsai PJ, et al. Visible-light-induced bactericidal activity of a nitrogen-doped titanium photocatalyst against human pathogens. *Appl Environ Microbiol*. 2006;72:6111-6.

[40] Foster HA, Ditta IB, Varghese S, Steele A. Photocatalytic disinfection using titanium dioxide: spectrum and mechanism of antimicrobial activity. *Applied Microbiology and Biotechnology*. 2011;90:1847-68.

[41] Mansoor A, Khurshid Z, Khan MT, Mansoor E, Butt FA, Jamal A, et al. Medical and Dental Applications of Titania Nanoparticles: An Overview. *Nanomaterials* (Basel). 2022;12.

[42] Fujishima A, Honda K. Electrochemical photolysis of water at a semiconductor electrode. *Nature*. 1972;238:37-8.

[43] Liou JW, Chang HH. Bactericidal effects and mechanisms of visible light-responsive titanium dioxide photocatalysts on pathogenic bacteria. *Arch Immunol Ther Exp* (Warsz). 2012;60:267-75.

[44] Sawada T, Yoshino F, Kimoto K, Takahashi Y, Shibata T, Hamada N, et al. ESR Detection of ROS Generated by TiO2 Coated with Fluoridated Apatite. *Journal of Dental Research.* 2010;89:848-53.

[45] Maness PC, Smolinski S, Blake DM, Huang Z, Wolfrum EJ, Jacoby WA. Bactericidal activity of photocatalytic TiO(2) reaction: toward an understanding of its killing mechanism. *Appl Environ Microbiol*. 1999;65:4094-8.

[46] Chen YL, Chen YS, Chan H, Tseng YH, Yang SR, Tsai HY, et al. The use of nanoscale visible light-responsive photocatalyst TiO2-Pt for the elimination of soil-borne pathogens. *PLoS One.* 2012;7:e31212.

[47] Buser D, Schenk RK, Steinemann S, Fiorellini JP, Fox CH, Stich H. Influence of surface characteristics on bone integration of titanium implants. A histomorphometric study in miniature pigs. *Journal of biomedical materials research*. 1991;25:889-902.

[48] Chernousova S, Epple M. Silver as antibacterial agent: ion, nanoparticle, and metal. *Angew Chem Int Ed Engl*. 2013;52:1636-53.

[49] Yin IX, Zhang J, Zhao IS, Mei ML, Li Q, Chu CH. The Antibacterial Mechanism of Silver Nanoparticles and Its Application in Dentistry. *Int J Nanomedicine*. 2020;15:2555-62.

[50] Sukumaran P, Poulose E. Silver nanoparticles: Mechanism of antimicrobial action, synthesis, medical applications, and toxicity effects. *International Nano Letters*. 2012;2.

[51] Ewald A, Glückermann SK, Thull R, Gbureck U. Antimicrobial titanium/silver PVD coatings on titanium. *Biomed Eng Online*. 2006;5:22.

[52] Besinis A, Hadi SD, Le HR, Tredwin C, Handy RD. Antibacterial activity and biofilm inhibition by surface modified titanium alloy medical implants following application of silver, titanium dioxide and hydroxyapatite nanocoatings. *Nanotoxicology.* 2017;11:327-38.

[53] Ágnes Veres LJ. Silver and Phosphate Functionalized Reactive TiO2/Polymer Composite Films for Destructions of Resistent Bacteria Using Visible Light. *Journal of Advanced Oxidation Technologies*. 2012;15.

[54] Tallósy SP, Janovák L, Ménesi J, Nagy E, Juhász Á, Dékány I. LED-light Activated Antibacterial Surfaces Using Silver-modified TiO2 Embedded in Polymer Matrix. *Journal of Advanced Oxidation Technologies*. 2014;17:9-16.

[55] Györgyey Á, Janovák L, Ádám A, Kopniczky J, Tóth KL, Deák Á, et al. Investigation of the *in vitro* photocatalytic antibacterial activity of nanocrystalline $TiO_2$ and coupled $TiO_2$/Ag

containing copolymer on the surface of medical grade titanium. *Journal of Biomaterials Applications.* 2016; 31:55-57.

[56] Venkei A, Ungvári K, Eördegh G, Janovák L, Urbán E, Turzó K. Photocatalytic enhancement of antibacterial effects of photoreactive nanohybrid films in an *in vitro* Streptococcus mitis model. *Arch Oral Biol.* 2020;117:104837.

[57] Belibasakis GN, Charalampakis G, Bostanci N, Stadlinger B. Peri-implant infections of oral biofilm etiology. *Adv Exp Med Biol*. 2015;830:69-84.

[58] Dhaliwal JS, Abd Rahman NA, Ming LC, Dhaliwal SKS, Knights J, Albuquerque Junior RF. Microbial Biofilm Decontamination on Dental Implant Surfaces: A Mini Review. *Front Cell Infect Microbiol*. 2021;11:736186.

[59] Monje A, Amerio E, Cha J-K, Kotsakis G, Pons Calabuig R, Renvert S, et al. Strategies for implant surface decontamination in peri-implantitis therapy. *International journal of oral implantology* (Berlin, Germany). 2022;15:213-48.

[60] Valderrama P, Blansett JA, Gonzalez MG, Cantu MG, Wilson TG. Detoxification of Implant Surfaces Affected by Peri-Implant Disease: An Overview of Non-surgical Methods. *Open Dent J*. 2014;8:77-84.

[61] Roos-Jansaker AM, Renvert S, Egelberg J. Treatment of peri-implant infections: a literature review. *J Clin Periodontol*. 2003;30:467-85.

[62] Dumitriu AS, Păunică S, Nicolae XA, Bodnar DC, Albu Ș D, Suciu I, et al. The Effectiveness of the Association of Chlorhexidine with Mechanical Treatment of Peri-Implant Mucositis. *Healthcare* (Basel). 2023;11.

[63] Prietto NR, Martins TM, Santinoni CDS, Pola NM, Ervolino E, Bielemann AM, et al. Treatment of experimental periodontitis with chlorhexidine as adjuvant to scaling and root planing. *Arch Oral Biol*. 2020;110:104600.

[64] Varoni E, Tarce M, Lodi G, Carrassi A. Chlorhexidine (CHX) in dentistry: state of the art. *Minerva Stomatol*. 2012;61:399-419.

[65] Marrelli M, Amantea M, Tatullo M. A comparative, randomized, controlled study on clinical efficacy and dental staining reduction of a mouthwash containing Chlorhexidine 0.20% and Anti Discoloration System (ADS). *Annali Di Stomatologia*. 2015;6:35-42.

[66] Eick S, Goltz S, Nietzsche S, Jentsch H, Pfister W. Efficacy of chlorhexidine digluconate-containing formulations and other mouthrinses against periodontopathogenic microorganisms. *Quintessence Int*. 2011;42:687-700.

[67] Liu JX, Werner J, Kirsch T, Zuckerman JD, Virk MS. Cytotoxicity evaluation of chlorhexidine gluconate on human fibroblasts, myoblasts, and osteoblasts. *J Bone Joint Infect.* 2018;3:165-72.

[68] Garcia-Sanchez A, Peña-Cardelles JF, Ordonez-Fernandez E, Montero-Alonso M, Kewalramani N, Salgado-Peralvo AO, et al. Povidone-Iodine as a Pre-Procedural Mouthwash to Reduce the Salivary Viral Load of SARS-CoV-2: A Systematic Review of Randomized Controlled Trials. *Int J Environ Res Public Health*. 2022;19.

[69] Bigliardi PL, Alsagoff SAL, El-Kafrawi HY, Pyon JK, Wa CTC, Villa MA. Povidone iodine in wound healing: A review of current concepts and practices. *Int J Surg*. 2017;44:260-8.

[70] Lachapelle JM. Allergic contact dermatitis from povidone-iodine: a re-evaluation study. *Contact Dermatitis*. 2005;52:9-10.

[71] Hoang T, Jorgensen MG, Keim RG, Pattison AM, Slots J. Povidone-iodine as a periodontal pocket disinfectant. *Journal of Periodontal Research.* 2003;38:311-7.

[72] Emrani J, Chee W, Slots J. Bacterial colonization of oral implants from nondental sources. *Clin Implant Dent Relat Res.* 2009;11:106-12.

[73] Noszticzius Z, Wittmann M, Kaly-Kullai K, Beregvari Z, Kiss I, Rosivall L, et al. Chlorine dioxide is a size-selective antimicrobial agent. *PLoS One*. 2013;8:e79157.

[74] Herczegh A, Gyurkovics M, Agababyan H, Ghidan A, Lohinai Z. Comparing the efficacy of hyper-pure chlorine-dioxide with other oral antiseptics on oral pathogen microorganisms and biofilm in vitro. *Acta Microbiol Immunol Hung*. 2013;60:359-73.

[75] Kerémi B, Márta K, Farkas K, Czumbel LM, Tóth B, Szakács Z, et al. Effects of Chlorine Dioxide on Oral Hygiene - A Systematic Review and Meta-analysis. *Curr Pharm Des.* 2020;26:3015-25.

[76] Yadav SR, Kini VV, Padhye A. Inhibition of Tongue Coat and Dental Plaque Formation by Stabilized Chlorine Dioxide Vs Chlorhexidine Mouthrinse: A Randomized, Triple Blinded Study. *J Clin Diagn Res*. 2015;9:69-74.

[77] Yeturu SK, Acharya S, Urala AS, Pentapati KC. Effect of Aloe vera, chlorine dioxide, and chlorhexidine mouth rinses on plaque and gingivitis: A randomized controlled trial. *J Oral Biol Craniofac Res.* 2016;6:54-8.

[78] Kotsakis GA, Lan C, Barbosa J, Lill K, Chen R, Rudney J, et al. Antimicrobial Agents Used in the Treatment of Peri-Implantitis Alter the Physicochemistry and Cytocompatibility of Titanium Surfaces. *Journal of Periodontology*. 2016;87:809-19.

[79] Park JB, Kim YK. Metallic biomaterials. In: The Biomedical Enginiering Handbook. 2nd ed. Vol. I. ed: *CRC Press and IEEE Press*, ISBN 0- 8493-0461-X, Boca Raton, Florida, USA.

[80] Kitano Y, Okada N. Separation of the epidermal sheet by dispase. *Br J Dermatol*. 1983;108:555-60.

[81] Mosmann T. Rapid colorimetric assay for cellular growth and survival: application to proliferation and cytotoxicity assays. *Journal of Immunological Methods*. 1983;65:55-63.

[82] Teixeira HS, Marin C, Witek L, Freitas A, Jr., Silva NR, Lilin T, et al. Assessment of a chair-side argon-based non-thermal plasma treatment on the surface characteristics and integration of dental implants with textured surfaces. *J Mech Behav Biomed Mater*. 2012;9:45-9.

[83] Kubies D, Himmlova L, Riedel T, Chanova E, Balik K, Douderova M, et al. The interaction of osteoblasts with bone-implant materials: 1. The effect of physicochemical surface properties of implant materials. *Physiol Res*. 2011;60:95-111.

[84] NIST X-ray photoelectron spectroscopy database v, Available from URL: http://srdata.nist.gov/xps/2003.

[85] Bereznai M, Pelsoczi I, Toth Z, Turzo K, Radnai M, Bor Z, et al. Surface modifications induced by ns and sub-ps excimer laser pulses on titanium implant material. *Biomaterials*. 2003;24:4197-203.

[86] Taranta A, Brama M, Teti A, De Luca V, Scandurra R, Spera G, et al. The selective estrogen receptor modulator raloxifene regulates osteoclast and osteoblast activity *in vitro*. *Bone*. 2002;30:368-76.

[87] Rampersad SN. Multiple applications of Alamar Blue as an indicator of metabolic function and cellular health in cell viability bioassays. *Sensors* (Basel). 2012;12:12347-60.

[88] Chan FK, Moriwaki K, De Rosa MJ. Detection of necrosis by release of lactate dehydrogenase activity. *Methods Mol Biol*. 2013;979:65-70.

[89] Ameen AP, Short RD, Johns R, Schwach G. The surface analysis of implant materials. 1. The surface composition of a titanium dental implant material. *Clin Oral Implants Res*. 1993;4:144-50.

[90] Sawase T, Hai K, Yoshida K, Baba K, Hatada R, Atsuta M. Spectroscopic studies of three osseointegrated implants. *J Dent*. 1998;26:119-24.

[91] Kilpadi DV, Raikar GN, Liu J, Lemons JE, Vohra Y, Gregory JC. Effect of surface treatment on unalloyed titanium implants: spectroscopic analyses. *J Biomed Mater Res*. 1998;40:646-59.

[92] Lausmaa J, Linder L. Surface spectroscopic characterization of titanium implants after separation from plastic-embedded tissue. *Biomaterials*. 1988;9:277-80.

[93] Wennerberg A, Albrektsson T. Effects of titanium surface topography on bone integration: a systematic review. *Clinical Oral Implants Research*. 2009;20 Suppl 4:172-84.

[94] Györgyey Á, Ungvári K, Kecskeméti G, Kopniczky J, Hopp B, Oszkó A, et al. Attachment and proliferation of human osteoblast-like cells (MG-63) on laser-ablated titanium implant material. *Materials Science & Engineering C, Materials for Biological Applications*. 2013;33:4251-9.

[95] Wennerberg A, Albrektsson T. Implant surfaces beyond micron roughness: Experimental and clinical knowledge of surface topography and surface chemistry. *Inter Dent SA*. 2006;8.

[96] Zhang Y, Gulati K, Li Z, Di P, Liu Y. Dental Implant Nano-Engineering: Advances, Limitations and Future Directions. *Nanomaterials* (Basel). 2021;11.

[97] Ivask A, Titma T, Visnapuu M, Vija H, Kakinen A, Sihtmae M, et al. Toxicity of 11 Metal Oxide Nanoparticles to Three Mammalian Cell Types *In Vitro*. *Current Topics in Medicinal Chemistry*. 2015;15:1914-29.

[98] Jeng HA, Swanson J. Toxicity of metal oxide nanoparticles in mammalian cells. *Journal of Environmental Science and Health Part A, Toxic/Hazardous Substances & Environmental Engineering*. 2006;41:2699-711.

[99] Riivari S, Närvä E, Kangasniemi I, Willberg J, Närhi T. Focal adhesion formation of primary human gingival fibroblast on hydrothermally and in-sol-made $TiO_{(2)}$ -coated titanium. *Clin Implant Dent Relat Res*. 2023;25:583-91.

[100] Azzawi ZGM, Hamad TI, Kadhim SA, Naji GA. Osseointegration evaluation of laser-deposited titanium dioxide nanoparticles on commercially pure titanium dental implants. *J Mater Sci Mater Med.* 2018;29:96.

[101] Mei S, Wang H, Wang W, Tong L, Pan H, Ruan C, et al. Antibacterial effects and biocompatibility of titanium surfaces with graded silver incorporation in titania nanotubes. *Biomaterials.* 2014;35:4255-65.

[102] Rossi S, Tirri T, Paldan H, Kuntsi-Vaattovaara H, Tulamo R, Närhi T. Peri-implant tissue response to $TiO_2$ surface modified implants. *Clinical Oral Implants Research*. 2008;19:348-55.

[103] De Giglio E, Cafagna D, Cometa S, Allegretta A, Pedico A, Giannossa LC, et al. An innovative, easily fabricated, silver nanoparticle-based titanium implant coating: development and analytical characterization. *Analytical and Bioanalytical Chemistry*. 2013;405:805-16.

[104] S. Moaddab, H. Ahari, D. Shahbazzadeh, A. A. Motallebi, A. Anva, J. Rahman-Nya, and M. R. Shokrgozar. Toxicity Study of Nanosilver (Nanocid®) on Osteoblast Cancer Cell Line. *Int. Nano lett*.2011:1, 11.

[105] Cameron SJ, Hosseinian F, Willmore WG. A Current Overview of the Biological and Cellular Effects of Nanosilver. *Int J Mol Sci*. 2018;19.

[106] Gherasim O, Puiu RA, Bîrcă AC, Burdușel AC, Grumezescu AM. An Updated Review on Silver Nanoparticles in Biomedicine. *Nanomaterials* (Basel). 2020;10.

[107] Ferraris S, Venturello A, Miola M, Cochis A, Rimondini L, Spriano S. Antibacterial and bioactive nanostructured titanium surfaces for bone integration. *Applied Surface Science*. 2014;311:279-91.

[108] Necula BS, van Leeuwen JP, Fratila-Apachitei LE, Zaat SA, Apachitei I, Duszczyk J. In vitro cytotoxicity evaluation of porous $TiO_2$-Ag antibacterial coatings for human fetal osteoblasts. *Acta Biomater*. 2012;8:4191-7.

[109] Tîlmaciu C-M, Mathieu M, Lavigne J-P, Toupet K, Guerrero G, Ponche A, et al. In vitro and in vivo characterization of antibacterial activity and biocompatibility: A study on silver-containing phosphonate monolayers on titanium. *Acta Biomaterialia*. 2015;15:266-77.

[110] Salaie RN, Besinis A, Le H, Tredwin C, Handy RD. The biocompatibility of silver and nanohydroxyapatite coatings on titanium dental implants with human primary osteoblast cells. *Mater Sci Eng C Mater Biol Appl*. 2020;107:110210.

[111] Smeets R, Precht C, Hahn M, Jung O, Hartjen P, Heiland M, et al. Biocompatibility and Osseointegration of Titanium Implants with a Silver-Doped Polysiloxane Coating: An *In Vivo* Pig Model. *Int J Oral Maxillofac Implants*. 2017;32:1338–45.

[112] Lampin M, Warocquier C, Legris C, Degrange M, Sigot-Luizard MF. Correlation between substratum roughness and wettability, cell adhesion, and cell migration. *J Biomed Mater Res.* 1997;36:99-108.

[113] J.I. Rosales-Leal MAR-V, G. Mazzagliaa, P.J. Ramón-Torregrosa,, L. Díaz-Rodríguez OG-M, M. Vallecillo-Capilla , C. Ruizc, M.A. Cabrerizo-Vílchez. Effect of roughness, wettability and morphology of engineered titanium surfaces on osteoblast-like cell adhesion. *Colloids and Surfaces A: Physicochem Eng Aspects*. 2010;365:222–9.

[114] Abushahba F, Tuukkanen J, Aalto-Setälä L, Miinalainen I, Hupa L, Närhi TO. Effect of bioactive glass air-abrasion on the wettability and osteoblast proliferation on sandblasted and acid-etched titanium surfaces. *Eur J Oral Sci*. 2020;128:160-9.

[115] Olvera-Huertas AJ, Costela-Ruiz VJ, García-Recio E, Melguizo-Rodríguez L, Illescas-Montes R, Reyes-Botella C, et al. The Effect of Chlorhexidine, Amoxicillin, and Clindamycin on the Growth and Differentiation of Primary Human Osteoblasts. *Int J Oral Maxillofac Implants*. 2022;37:283-8.

[116] Almazin SM, Dziak R, Andreana S, Ciancio SG. The effect of doxycycline hyclate, chlorhexidine gluconate, and minocycline hydrochloride on osteoblastic proliferation and differentiation *in vitro. J Periodontol.* 2009;80:999-1005.

[117] Kozlovsky A, Artzi Z, Moses O, Kamin-Belsky N, Greenstein RB. Interaction of chlorhexidine with smooth and rough types of titanium surfaces. *J Periodontol*. 2006;77:1194-200.

[118] Patil C, Agrawal A, Abullais SS, Arora S, Khateeb SU, Fadul AEM. Effectiveness of Different Chemotherapeutic Agents for Decontamination of Infected Dental Implant Surface: A Systematic Review. *Antibiotics* (Basel). 2022;11.

[119] Ernest EP, Machi AS, Karolcik BA, LaSala PR, Dietz MJ. Topical adjuvants incompletely remove adherent Staphylococcus aureus from implant materials. *J Orthop Res*. 2018;36:1599-604.

[120] Taha M, Arulanandam R, Chen A, Diallo JS, Abdelbary H. Combining povidone-iodine with vancomycin can be beneficial in reducing early biofilm formation of methicillin-resistant Staphylococcus aureus and methicillin-sensitive S. aureus on titanium surface. *J Biomed Mater Res B Appl Biomater*. 2023;111:1133-41.

[121] Venkei A, Eördegh G, Turzó K, Urbán E, Ungvári K. A simplified in vitro model for investigation of the antimicrobial efficacy of various antiseptic agents to prevent peri-implantitis. *Acta Microbiol Immunol Hung*. 2020;67:127-32.

[122] Barrak I, Baráth Z, Tián T, Venkei A, Gajdács M, Urbán E, et al. Effects of different decontaminating solutions used for the treatment of peri-implantitis on the growth of Porphyromonas gingivalis-an in vitro study. *Acta Microbiol Immunol Hung*. 2020.1,40-47.

[123] Kabata T, Maeda T, Kajino Y, Hasegawa K, Inoue D, Yamamoto T, et al. Iodine-Supported Hip Implants: Short Term Clinical Results. *Biomed Res Int*. 2015;2015:368124.

[124] Ma JW, Huang BS, Hsu CW, Peng CW, Cheng ML, Kao JY, et al. Efficacy and Safety Evaluation of a Chlorine Dioxide Solution. *Int J Environ Res Public Health*. 2017;14.